Journal of Sound and Vibration

Control of Rayleigh wave propagation through imposing Mindlin boundary conditions on the surface --Manuscript Draft--

Manuscript Number:	JSV-D-21-01916R1
Article Type:	Full Length Article
Section/Category:	B Passive control of sound and vibration
Keywords:	Rayleigh wave control; Elastodynamic resonant metasurface; Mindlin boundary conditions; mode conversions; frequency-domain analysis; time-domain analysis
Corresponding Author:	Parisa Shokouhi The Pennsylvania State University University Park, UNITED STATES
First Author:	Lalith Sai Srinivas Pillarisetti
Order of Authors:	Lalith Sai Srinivas Pillarisetti
	Cliff J Lissenden
	Parisa Shokouhi
Abstract:	A resonant metasurface design based on boundary condition (BC) manipulation was recently established to control low-frequency Lamb waves in a plate. This study identifies the necessary BCs that forbid Rayleigh wave propagation in order to find a rational design methodology for an optimized BC-controlled meta-surface. An analytical study of Mindlin BCs, a type of Cauchy BCs, shows promise in surface wave control. The frequency-domain and time-domain finite element studies performed by imposing Mindlin BCs in the path of Rayleigh wave propagation are consistent with analytical predictions, exhibiting no Rayleigh wave transmission. The simulations reveal mode conversions from Rayleigh wave to bulk waves directed into the half-space and a low amplitude Rayleigh wave reflection. For a finite-sized BC patch, the radial beam spreading of the mode-converted bulk waves keeps some energy near the surface, which could convert back to Rayleigh waves at the end of the BC patch. Thus, the BC patch must be sufficiently long to effectively suppress surface waves. Finally, we show that the Mindlin BCs can be imposed by a rod-like prismatic resonator at the resonator's longitudinal frequency. These findings provide new insights into the coupling that promotes surface wave control, potentially leading to novel metasurface designs.



Parisa Shokouhi, Ph.D., P.E. Associate Professor of Engineering Science and mechanics College of Engineering (814) 863-0678

The Pennsylvania State University 212 Earth and Engineering Sciences Building University Park, PA 16802

September 15, 2021

Dear Editor,

We are submitting our manuscript titled "Control of Rayleigh wave propagation through imposing Mindlin boundary conditions on the surface" for your consideration and publication in the *Journal of Sound and Vibration*.

In this work, we report the efficacy of a particular type of Cauchy boundary conditions (BC), called Mindlin BCs, in preventing Rayleigh wave propagation. We demonstrate that imposing the Mindlin BCs on the surface results in the conversion of the incident Rayleigh wave to bulk waves directed away from the surface. Besides, a low-amplitude reflected Rayleigh wave, which accounts for 7% of the incident wave amplitude, is observed. The interaction of Rayleigh waves with the Mindlin BC region is analyzed using frequency-domain and time-domain finite element simulations together with wavenumber spectrum analysis. We provide a parametric study using FDFE simulations to find the minimum required length of the Mindlin BC patch to significantly block Rayleigh wave propagation. We also discuss on the wave propagation angles of the mode-converted bulk waves, the presence of multiple mode conversions for a finite-sized Mindlin BC patch, and an example showing how a prismatic rod-like resonator can impose Mindlin BCs on an elastic half-space surface.

To our knowledge, this is the first study that provides an insight into the use of Mindlin BCs for a BC-controlled meta-surface design to manipulate Rayleigh waves. The reported findings on the mode-conversions of the incident Rayleigh wave when encountering imposed Mindlin BCs on the surface are unique and will lead to novel resonator design strategies. We believe that our research results have broad applications across length scales e.g., in seismic isolation of structures, vibration control, and designing surface acoustic wave (SAW) devices.

Below we list several qualified, potential referees (in alphabetical order):

- Andrea Colombi (colombi@ibk.baug.ethz.ch)
- Antonio Palermo (antonio.palermo6@unibo.it)
- Alessandro Marzani (alessandro.marzani@unibo.it)

Best Regards,

Parisa Shokouhi

Parisa Shokouhi, on behalf of all co-authors.

Highlights (for review)

Highlights:

- 1. Mindlin boundary conditions (BCs) show promise for Rayleigh wave suppression
- 2. Rayleigh waves incident on Mindlin BCs decouple to its bulk wave components
- 3. The incident Rayleigh waves partially recover post a short Mindlin BC patch
- 4. Effective suppression of Rayleigh waves requires a long Mindlin BC patch
- 5. Rod-like resonators impose Mindlin BCs at their longitudinal resonance frequencies

Response to reviewers

The authors thank the reviewers for a detailed review of our manuscript and providing constructive and valuable feedback. All the reviewers' comments are addressed, and the changes made to the manuscript are highlighted for your reference.

Reviewer #1:

The manuscript describes a, primarily numerical, study on the interaction between Rayleigh waves on elastic half-planes and some classical and non-classical boundary conditions. Although the paper makes no attempt to justify the non-classical boundary conditions, I note that they can be justified on physical grounds. The authors demonstrate that a single rod-like resonator, at resonance, can emulate the effect of imposing a Mindlin boundary condition. As pointed out by the authors, the junction conditions between the rod and half-plane will play an important role — this problem is highly non-trivial.

I have carefully read the manuscript several times and can find no material errors or omissions. The work is interesting, rigorous, and well done. I am therefore happy to recommend publication in its present form.

The authors thank the reviewer for recommending the publication of the manuscript without any further changes.

Reviewer #2:

This paper presents a Rayleigh-wave control analysis via applying the so-called Mindlin BC on a half-space surface. In doing so, the authors quickly review the effect of different BCs on the propagation of Rayleigh waves and then conduct an FE analysis of a finite-size Mindlin BC. Although Rayleigh wave manipulation via metasurfaces is an active topic in JSV, the Reviewer suggests declining this paper due to the following reasons.

1. The paper is not well written. In particular, the flow is not concise and precise. For example, in the first paragraph of the introduction, all the rest except the last sentence is common sense to the audience of this journal. The second paragraph jumps to a review of the literature on phononic crystals and metamaterials, and does not return to a review of the literature on Rayleigh wave modulation until the third paragraph.

Thank you for your comments. Our argument to the first point is that the article can't start with that last sentence in the first paragraph. We tried to provide some perspective and context for our contribution. From your comment we infer that you do not need this perspective, but we argue that many readers less familiar with the topic will appreciate it.

The authors have structured the flow of the first paragraph to suggest the implications of this research across length scales; in seismic isolation of structures, vibration control, and designing surface acoustic wave (SAW) devices. The second paragraph introduces elastodynamic metamaterials and motivates the resonant metamaterials; it includes a brief distinction between the local resonance-based and Bragg scattering-based metamaterials for less familiar readers before diving into the literature focused on suppressing Rayleigh waves in the following paragraph.

2. In the introduction, this work does not clearly identify the research gap, the innovation, or the novelty. Particularly, the statement "...understanding the coupling between the resonator and the base material is not yet fully explored" in the fourth paragraph is not really true. Instead, the physics of this problem has been well understood, see, for example, Boechler et.al PRL 2013, Colquitt et.al JMPS 2017.

The authors agree with the reviewer that some aspects of the physics concerning the interaction of a periodic arrangement of prismatic rods with the Rayleigh wave propagation is well studied in [23] by solving the complex boundary value problem. However, an explanation for the mode-conversion of Rayleigh wave to shear waves is not explicitly provided. Moreover, the coupling conditions (vertical force exerted by the resonator rod on the half-space) derived in [23] is valid for the case of a prismatic rod but cannot be generalized for an arbitrary resonator geometry. This paper provides a new perspective of the same problem by demonstrating that Mindlin BCs (vertical displacement is clamped at the resonator base) are imposed at the fixed-free longitudinal eigenfrequency of the resonator, justifying the mode-conversion of the incident Rayleigh wave to shear wave (Lines: 489-494). Analogous to imposing Mindlin BCs by a prismatic resonator, resonators with non-intuitive geometries which impose Mindlin BCs at desired frequencies are possible through topology optimization and are the subject of a future manuscript.

Understanding the interaction of Rayleigh waves with Mindlin BCs (finite/infinite sized) is a vital step for realizing BC-based resonator designs. And this is the knowledge gap that the authors would like to fill with this paper, as indicated in lines 81-88:

"Though the periodic insertion of the cylindrical [33], cubic [34], and rod-like [28] resonators created band gaps to control Rayleigh wave propagation, the coupling between the resonator and the base material is not exploited in the design of the resonators.

This paper extends the approach of Lissenden et al. to identify the BCs that help suppress Rayleigh surface waves. This is a fundamental step towards realizing a BC-controlled resonant metasurface design for blocking Rayleigh surface waves in a linear elastic half-space."

The authors argue that analyzing the mode conversions (first and second) of the Rayleigh wave incidence on Mindlin BCs patches is nontrivial and has potential implications for optimized resonator designs. Our research team is currently working on this topology optimization methodology to design optimized resonators that emulate Mindlin BCs on the half-space. The parametric study using different BC patch lengths provides inputs into the dimensions of the design domain for topology optimization to enhance Rayleigh wave suppression with fewer resonators.

The authors, however, accept the reviewer's suggestion and modify the statement to be more specific on the implications and applications of this paper's findings:

"Though the periodic insertion of the cylindrical [33], cubic [34], and rod-like [28] resonators created band gaps to control Rayleigh wave propagation, the coupling between the resonator and the base material is not exploited in the design of the resonators."

3. In section 2, the Neumann BCs and Dirichlet BCs results can be found in any of the relevant textbooks, so there is no need to list them again.

The authors agree that the Neumann BCs and Dirichlet BCs results are well known to the scientific community. However, the authors feel that including these results provides a better flow of passage for the reader before describing the two novel results of Mindlin and Auld BCs. Considering this comment, we have removed some details for brevity.

Lines: 140-145:

"Imposing the Neumann (traction-free) BCs ($\sigma_{33} = \sigma_{13} = 0$) on the surface of the half-space results in the well-known Rayleigh surface waves [37], whereas imposing the Dirichlet BCs ($u_1 = u_3 = 0$) results in nondispersive surface waves [35] that propagate with a phase speed of $c = \sqrt{c_L^2 + c_T^2}$. Next, let us evaluate the possible surface wave solutions for the following Cauchy type BCs that are of interest to this study:"

4. Although some interesting phenomena were provided via simulations, such as surface-to-bulk conversion that are usually present in elastic metasurfaces, this work lacks a clear and precise explanation of the physical mechanism induced by the Mindlin BC.

The authors have demonstrated that a half-space with Mindlin BCs imposed on the surface possess no surface wave solutions. This explains the delocalization of the Rayleigh wave propagating on a traction-free surface to longitudinal and transverse waves upon encountering Mindlin BCs, as these are the only wave solutions that exist. As demonstrated in lines 150-152:

"This BC was initially proposed by Mindlin [38] to decouple the longitudinal (L) and shear vertical (SV) wave modes in isotropic plates and was later extended by Solie and Auld for anisotropic plates [39]."

Mindlin BCs have shown a similar decoupling of the shear and dilatational behavior for guided modes propagating in an elastic plate.

Our numerical study provides an in-depth understanding of all the possible mode-conversions and the extent of Rayleigh wave reflection when a Rayleigh wave is incident on Mindlin BCs. We choose a numerical study as the mode conversions (first and second for a finite-sized patch) could be easily visualized providing deeper insights into the design of novel metamaterials. Moreover, the proposed numerical study helps analyze the influence of BC patch length on the extent of delocalization of Rayleigh waves to bulk waves. This numerical method could be extended for an array of equally spaced Mindlin BC patches to study the influence of patch length and spacing. This study could help optimize the performance of a meta-surface composed of prismatic resonators to achieve wider bandgaps without the need for full-scale simulations with resonators. As explained in lines 443-444:

"Future studies will include a careful study of Rayleigh reflection and refraction due to the imposed BCs to better understand the reported observations here."

future studies will include solving analytically the Mixed BC problem of the Rayleigh wave incident on Mindlin BCs to understand better the reported numerical observations.

5. The authors argued that the Mindlin BC can be imposed by a rod-like resonator. However, the Mindlin BC in this paper is: \sigma_{13} =0, u_3 = 0 for x_3 = 0, while the effective BC of rod-like resonators is \sigma_{13} =0, \sigma_{33} =Z\times u_3, where Z is the impedence function, see: Supplementary Materials for A seismic metamaterial: The resonant metawedge. From this point of view they are different.

The comparison between Mindlin BC and rods should be considered via a collection of resonators rather than one in the discussion part.

The authors argue that both these BC representations are true. It has been shown in [23,7] that the vertical force exerted per unit area of the resonator on the half-space as:

$$V(\omega) = A\omega\sqrt{E\rho}\tan\left(Lw\sqrt{\frac{\rho}{E}}\right)$$

where E, ρ and L are the Youngs modulus, density, and length of the resonator and ω is the angular frequency. It can be demonstrated that the clamping of the vertical displacement at the resonator base occurs (See the figure below) at the resonator's longitudinal resonance frequency from a simple frequency domain analysis of the resonator with the forcing function $V(\omega)$ applied to the resonator base. This indicates that Mindlin BCs are imposed at the longitudinal resonance frequency.

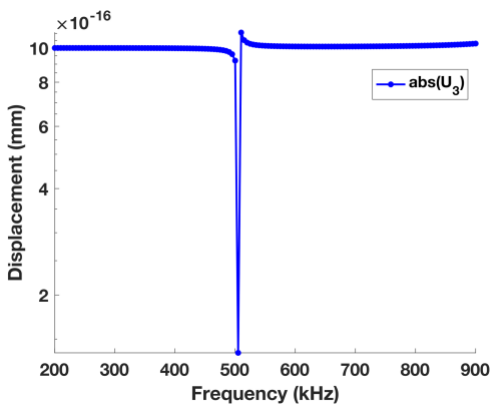


Fig: Displacement profile (abs(U₃)) extracted at the base of the prismatic resonator under the forced excitation (V(ω)) of the resonator base. The dip in the profile indicates clamping of the vertical displacement at the longitudinal resonance frequency

The imposed Mindlin BCs convert the incident Rayleigh wave to bulk waves (predominantly shear) as demonstrated in the paper through the frequency-independent patch studies. The authors have modified the discussion section to add these details (lines 489-494):

"Though the physics behind Rayleigh wave interaction with the prismatic rods (considering only the longitudinal motion of resonators) is demonstrated analytically in [23] by solving the boundary value problem, the explanation to the mode-conversion of Rayleigh wave to shear waves is not explicitly detailed. This analysis provides an insight into the mechanism that leads to the conversion of Rayleigh waves to the bulk waves using prismatic resonators."

As explained in response to the previous comment, the above forcing function is valid for the case of a prismatic rod but cannot be generalized for an arbitrary resonator geometry. Thus, this paper provides a new perspective on the same problem by demonstrating that Mindlin BCs (vertical displacement is clamped at the resonator base) are imposed at the fixed-free longitudinal eigenfrequency of the resonator that can be conveniently exploited for designing optimized resonators of arbitrary geometry, as explained in lines 520-524 and 557-559:

[&]quot;Although designing resonators based on longitudinal resonance frequency matching is straightforward, matching the BCs at the resonator base at prescribed frequencies could provide further insights into how the bandgaps are created leading to novel metasurface designs."

[&]quot;Analogous to the clamping of the vertical displacement by a prismatic resonator, non-intuitive resonator designs are possible through topology optimization that imposes Mindlin BCs at desired frequencies."

The authors would like to reiterate that a prismatic resonator of a small width results in lesser mode conversion of Rayleigh wave to bulk waves. It was demonstrated that this limitation arises due to the second mode conversion, where a part of the transverse wave mode converts back to Rayleigh wave (lines: 494-499). Therefore, achieving significant Rayleigh wave suppression requires an array of prismatic resonators. This can be confirmed by comparing the frequency domain simulations at 510 kHz frequency for an array of resonators with an array of Mindlin BC patches of similar dimensions as the resonator base. An array of resonators readily suppresses the Rayleigh wave with each Mindlin BC patch (imposed by the resonators) successively converting a part of the Rayleigh wave to the shear waves.

Based on the reviewer's suggestion, the authors have also included a study on an array of prismatic resonators in the discussion section to demonstrate the imposing of Mindlin BCs by all the resonators. Please refer to the lines 506-519 and Fig. 14 in the document for the modifications:

"The FDFE analysis performed on a single resonator (Fig. 12(a)) can be extended to an array of 30 resonators to confirm the imposing of Mindlin BCs by all the resonators at the longitudinal resonance frequency. To demonstrate this, we compare the displacement fields resulting from the interaction of the Rayleigh wave with an array of resonators (Fig. 14(a)) and an array of an equal number of (frequency-independent) Mindlin BC patches (Fig. 14(b)) at 510 kHz (longitudinal resonance frequency of the resonator). The dimensions of each Mindlin BC patches is considered 1.4 mm ($\sim \lambda_R/4$). The displacement fields (Re(U₃)) for both the cases (resonators/patches) are very similar and show enhanced suppression of Rayleigh waves (90% suppression). These results indicate that an array of resonators impose an array of Mindlin BC patches (at 510 kHz) and thereby provide significant Rayleigh wave suppression"

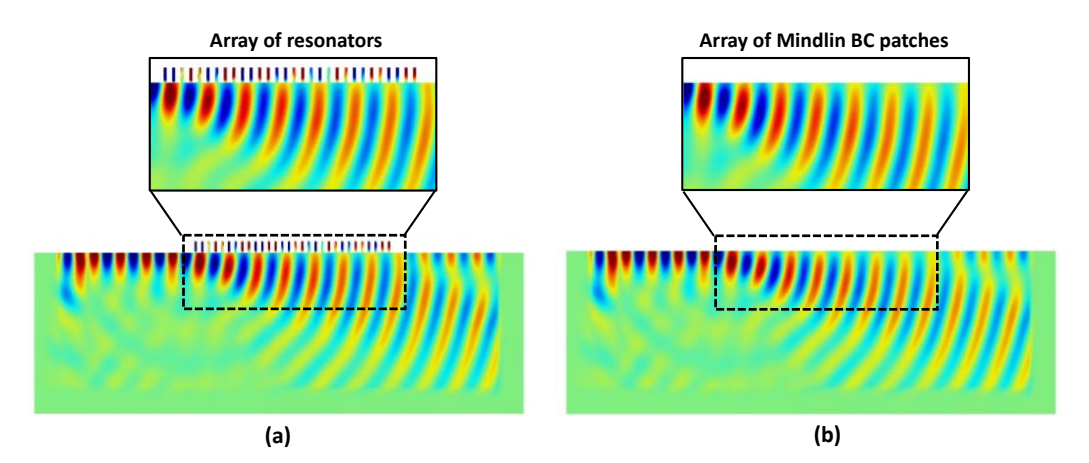


Fig. 14: (a) Displacement fields (Real(U₃)) obtained for the cases with (b) an array of 30 resonators, each having their first longitudinal resonance frequency at 510 kHz and (c) an array of frequency-independent Mindlin BC patches. The cut outs in subfigures (a) and (b) provide an enlarged view of the resonator and the near-surface `incident" and `transmitted" regions.

6. In the abstract the authors stated that "These findings provide new insights into the coupling that promotes surface wave control, potentially leading to novel metasurface designs". To the reviewer, the paper doesn't really match the premise of this statement.

Thanks for your comment, but the authors do not agree with the reviewer's assessment that the findings in this paper do not justify the premise of the statement stated in the abstract.

Studying the interaction of the Rayleigh wave with the Mindlin BC patch (infinite/finite-sized) is a non-trivial problem, which has not bene attempted before. As explained in the introduction, such a study is required to design optimized resonators that impose Mindlin BCs to suppress Rayleigh wave propagation. The authors study this interaction with the Mindlin BC patch through an extensive finite element analysis. The mode conversions (first and second) involved during the interaction provide a perspective of why a single prismatic resonator cannot suppress the Rayleigh wave and why an array of resonators does (Lines: 494-518). We demonstrate an intuitive example of a prismatic resonator imposing Mindlin BCs under Rayleigh wave propagation to draw a connection between frequency-independent Mindlin BC patch studies and a frequency-dependent Mindlin BC patch imposed by the resonator.

As explained earlier, analogous to imposing Mindlin BCs by a prismatic resonator, topology optimization can be used to design resonators with non-intuitive geometries, which impose Mindlin BCs at desired frequencies. The authors have modified the discussion/conclusion section to highlight these details:

Lines 520-524:

"Although designing resonators based on longitudinal resonance frequency matching is straightforward, matching the BCs at the resonator base at prescribed frequencies could provide further insights into how the bandgaps are created leading to novel metasurface designs."

Lines 557-559:

"Analogous to the clamping of the vertical displacement by a prismatic resonator, non-intuitive resonator designs are possible through topology optimization that imposes Mindlin BCs at desired frequencies."

The design methodology for the BC-matched resonators will be discussed in detail in our upcoming manuscript as the authors would like to focus the current paper more on identifying the BCs responsible for suppressing surface waves.

The study presented in this paper advances our understanding of the coupling conditions responsible for Rayleigh wave suppression and mode conversion, motivating the design of BC-matched resonator designs. Therefore, in our opinion, the findings of this paper clearly justify the premise of the statement stated in the abstract.

Reviewer #3:

The authors provide an interesting insight into manipulation of surface waves via boundary condition design. Based on the theoretical analysis, they find that Mindlin BCs cannot support the transmission of surface waves, owing to which the incident Rayleigh waves will transfer into bulk waves. Both frequency-domain and time-domain simulations are conducted to illustrate the mode-conversion from Rayleigh waves to bulk waves. Finally, they try to reveal the mechanism of band gaps caused by surface pillars from the view of BC types. This paper is valuable and may provide a novel insight into the design/mechanism of metasurface.

1. It will be better if they can give a deeper discussion on how to use the wave phenomena with respect to ideal/classical boundary conditions to guide the design of micro-structures to mimic the results.

Thank you for the comment. In this paper, the authors would like to focus more on the interaction of Rayleigh wave propagation with frequency-independent Mindlin BCs and its implications. We demonstrate an example of a prismatic resonator imposing Mindlin BCs during Rayleigh wave propagation to draw a connection between frequency-independent Mindlin BC patch studies and a frequency-dependent Mindlin BC patch imposed by the resonator.

Analogous to the clamping of the vertical displacement by a prismatic resonator, non-intuitive resonator designs are possible through topology optimization that impose Mindlin BCs at desired frequencies. The authors have modified the discussion/conclusion section to highlight these details:

Lines 489-494

"Though the physics behind Rayleigh wave interaction with the prismatic rods (considering only the longitudinal motion of resonators) is demonstrated analytically in [23] by solving the boundary value problem, the explanation to the mode-conversion of Rayleigh wave to shear waves is not explicitly detailed. This analysis provides an insight into the mechanism that leads to the conversion of Rayleigh waves to the bulk waves using prismatic resonators."

Lines 520-524:

"Although designing resonators based on longitudinal resonance frequency matching is straightforward, matching the BCs at the resonator base at prescribed frequencies could provide further insights into how the bandgaps are created leading to novel metasurface designs."

Lines 557-559:

"Analogous to the clamping of the vertical displacement by a prismatic resonator, non-intuitive resonator designs are possible through topology optimization that imposes Mindlin BCs at desired frequencies."

The authors feel that the modified discussion of prismatic resonators provides sufficient insight into how these Mindlin BCs can be exploited towards designing non-intuitive resonators using topology optimization. The design methodology for these BC-matched resonators will be discussed in detail in our upcoming manuscript.

2. Local resonance of the pillar maybe a case of the Mindlin BC, but it is not a good one owing to the narrow bandgap width.

A minor suggestion: The influence of the Mindlin BC length should be further analyzed by parameter study, a relation between the BC length and the transfer ratio of the mode conversion should be presented, and the critical length that makes good mode conversion should also be defined.

The authors agree with the reviewer's comments. As the reflected Rayleigh wave is independent of the patch length, the transmission ratio could quantify the extent of Rayleigh wave mode conversion to bulk waves. This has been added to the discussion in lines 390-393.

"As the reflected Rayleigh wave is independent of the patch length, the amount of Rayleigh wave suppression achieved quantitatively represents the extent of mode-conversion of Rayleigh waves to bulk waves"

The authors have explicitly stated that the complete Rayleigh wave suppression (~99%) requires Mindlin BC patch length to be 10 times greater than the Rayleigh wavelength (lines: 384-387), and this is therefore the critical length for maximum mode-conversion.

As described in the discussion section, it is impractical to achieve a Mindlin BC patch length more than a Rayleigh wavelength using prismatic resonators due to the constraint over the resonator length to match the longitudinal resonance frequency with the incident Rayleigh wave frequency (lines: 494-499). However, the parametric study presented in this manuscript with different Mindlin BC patch lengths provides key inputs for the BC-optimized resonator design methodology (through topology optimization) to enhance Rayleigh wave suppression with fewer resonators, thereby enhancing the bandgap.

Additionally, the use of an array of resonators seems to be much more effective than enlarging the size of a single resonator as illustrated by the new Fig. 14. While in this article the objective is to understand the BC coupling between half-space and resonator, the applications of interest to the authors will likely contain an array of resonators.

Control of Rayleigh wave propagation through imposing Mindlin boundary conditions on the surface

Lalith Sai Srinivas Pillarisetti^a, Cliff J Lissenden^a, Parisa Shokouhi^a

^aDepartment of Engineering Science and Mechanics, Penn State, University Park, Pennsylvania 16802, USA

Abstract

A resonant metasurface design based on boundary condition (BC) manipulation was recently established to control low-frequency Lamb waves in a plate. This study identifies the necessary BCs that forbid Rayleigh wave propagation in order to find a rational design methodology for an optimized BCcontrolled meta-surface. An analytical study of Mindlin BCs, a type of Cauchy BCs, shows promise in surface wave control. The frequency-domain and timedomain finite element studies performed by imposing Mindlin BCs in the path of Rayleigh wave propagation are consistent with analytical predictions, exhibiting no Rayleigh wave transmission. The simulations reveal mode conversions from Rayleigh wave to bulk waves directed into the half-space and a low amplitude Rayleigh wave reflection. For a finite-sized BC patch, the radial beam spreading of the mode-converted bulk waves keeps some energy near the surface, which could convert back to Rayleigh waves at the end of the BC patch. Thus, the BC patch must be sufficiently long to effectively suppress surface waves. Finally, we show that the Mindlin BCs can be imposed by a rod-like prismatic resonator at the resonator's longitudinal frequency. These findings provide new insights into the coupling that promotes surface wave control, potentially leading to novel metasurface designs.

Keywords: Rayleigh wave control, Elastodynamic resonant metasurface,

^{*}Parisa Shokouhi Email address: parisa@psu.edu (Parisa Shokouhi)

Mindlin boundary conditions, Mode conversions, frequency-domain analysis, and time-domain analysis

1. Introduction

Rayleigh waves are elastic surface waves that travel along the surface of a traction-free isotropic elastic half-space. The out-of-phase horizontal and vertical displacement components of the Rayleigh wave result in an elliptical motion that decays exponentially with depth. Rayleigh waves are encountered over a wide range of frequencies. The low-frequency (~ 0.1 -10 Hz) Rayleigh waves emitted during earthquakes and explosions can be destructive even at long distances from the source. The mid-frequency (~100 Hz) Rayleigh waves generated by traffic loading and other human activities could harm sensitive instruments and machinery in the nearby industrial sites [1]. Rayleigh waves at 0.01-10 MHz frequency are widely used in nondestructive evaluation (NDE). Furthermore, the high-frequency Rayleigh waves in the MHz to GHz range are exploited in the design of surface acoustic wave (SAW) devices that are extensively used in various electronic and biomedical applications, such as delay lines, filters, transducers, and sensors [2, 3]. Therefore, controlling Rayleigh surface wave propagation has broad applications across length scales ranging from seismic isolation of structures and vibration control to the design optimization of miniature electronic devices.

In the past two decades, there has been a significant advancement in research towards elastodynamic metamaterials for applications in controlling elastic waves. These are engineered composite materials with unusual material properties such as negative effective mass density and elastic modulus that enable elastic wave manipulation in non-intuitive ways. Many previous investigations involved focusing [4, 5], steering [6], mode-filtering [7, 8], and cloaking [9, 10, 11] of the incident elastic waves by exploiting these unnatural properties of metamaterials. Analogous to photonic crystals used in electromagnetic applications, phononic crystals are a class of elastodynamic metamaterials that exploit Bragg

scattering within the periodically ordered substructure to create stop-band gaps to control wave propagation [12]. However, this requires the periodicity of the substructure to match the wavelength of the incident wave, making phononic crystals unfavorable for low-frequency applications. In contrast, locally resonant metamaterials employ a periodic or random arrangement of subwavelength resonators to create stop-band gaps, thereby easing the requirement of unit-cell periodicity to be comparable to the wavelength [13, 14, 15]. Unlike phononic crystals, the band gaps in locally resonant metamaterials are achieved through the hybridization between the incident plane waves and the local resonance of the resonators [13, 16, 17].

Early studies to control Rayleigh wave propagation using the concept of phononic crystals include periodically distributed cylindrical holes in the host medium with stop-band gaps resulting from Bragg scattering of the incident Rayleigh wave by air holes [18, 19]. On the other hand, locally resonant metamaterials using a two-dimensional array of pillars erected on a semi-infinite substrate have been shown numerically [20] and experimentally [21] to create stopband gaps at frequencies significantly lower than that can be achieved through Bragg scattering. Such two-dimensional surface arrays of resonators used to manipulate the incident waves using local resonance phenomena were later termed "metasurfaces" [22, 23]. Analytical derivation of the Rayleigh wave dispersion due to the local resonances of the surface-mounted damped harmonic oscillators was first provided by Garova et al [24]. Palermo et al. proposed a seismic metasurface using the near-surface buried sub-wavelength cylindrical resonators to convert Rayleigh waves to shear waves that propagate away from the surface [25, 22]. Miniaci et al. performed a parametric study on the Bragg scattering and local-resonance-based cylindrical borehole metamaterial designs using a 3D large-scale dispersion and finite-element analysis [26]. At the microscopic scale, silica microspheres adhered to a silica substrate was shown to exhibit hybridization between the contact resonance of the microspheres with the surface acoustic waves [27]. Several investigations by Colombi et al. concern a metasurface comprising surface-mounted rods that support both flexural and compressional

resonances [28, 7, 29]. Their studies included designing a resonant meta-wedge capable of trapping and mode-converting the incident Rayleigh waves over a broad frequency range. The formation of stop-band gaps for Rayleigh waves using resonant rods was attributed to the hybridization or Fano interferences between the Rayleigh wave and the local longitudinal resonances of the rods [23].

Most studies employed parametric study-based resonator design requiring extensive numerical analysis to optimize the geometrical and material properties of the unit cell [26]. Recently, Lissenden et al. provided a novel boundary condition (BC)-based approach for designing resonant metasurface to forbid the propagation of low-frequency Lamb waves in a plate [30]. They attributed the formation of hybridization stop-band gaps to imposing particular Cauchytype BCs to the resonator base. They demonstrated that blocking the incident A0 Lamb waves in the plate could be achieved by imposing Mindlin BCs on the surface of the plate at the resonator's anti-resonant frequency, matching the frequency of incident A0 Lamb waves. Similarly, blocking S0 Lamb waves is possible through applying Auld BCs between the plate and the resonator. These BC-controlled resonant metasurface designs agree well with the rod-like resonators employed by Rupin et al. [31] to control A0 waves and the clamping four-arm resonators used by Hakoda et al. [32] to control S0 wave propagation. The BC-controlled metasurface design is novel in that it decouples the resonator design from the wave propagation and provides new insights to control elastic wave propagation. Though the periodic insertion of the cylindrical [33], cubic [34], and rod-like [28] resonators created band gaps to control Rayleigh wave propagation, the coupling between the resonator and the base material is not exploited in the design of the resonators.

This paper extends the approach of Lissenden *et al.* to identify the BCs that help suppress Rayleigh surface waves. This is a fundamental step towards realizing a BC-controlled resonant metasurface design for blocking Rayleigh surface waves in a linear elastic half-space. An analytical study performed to investigate the influence of various BCs (applied to the surface of a half-space) on

Rayleigh wave propagation suggests the efficacy of Mindlin BCs for suppressing the incident Rayleigh waves. This is further validated through extensive numerical analyses. These BCs represent the necessary continuity conditions between the resonator and the surface of the elastic half-space, thus, advancing our understanding of the coupling between the resonator and the half-space required to suppress Rayleigh wave propagation. Knowing the necessary BCs and the minimum required length of the 'BC manipulation region', one can design resonators that impose these BCs on the surface to effectively block Rayleigh wave propagation.

The remainder of the paper is arranged as follows. Section 2 provides an analytical study of the possible surface-wave solutions in an elastic half-space with different BCs. The efficacy of Mindlin BCs in suppressing Rayleigh wave propagation is demonstrated in Section 3 with extensive frequency-domain and time-domain finite element simulations. Section 4 illustrates the influence of the Mindlin BC patch length on the incident Rayleigh waves. Finally, a discussion of the results is provided in Section 5 include the wave propagation angles of the mode-converted waves, the presence of multiple mode conversions for a finite-sized Mindlin BC patch, and examples showing how prismatic rod-like resonators can impose Mindlin BCs on an elastic half-space surface.

2. ANALYTICAL STUDY: INFLUENCE OF BOUNDARY CON-DITIONS ON RAYLEIGH WAVE PROPAGATION

Similar to what is recently shown for low-frequency Lamb wave propagation [30], manipulating the BCs on the surface of an elastic half-space can significantly affect the Rayleigh surface wave propagation. However, to the best of the authors' knowledge, there is no comprehensive study of the BC effects on surface wave propagation. This section provides an analytical framework to study the influence of Neumann, Dirichlet, and a pair of Cauchy BCs on the surface wave propagation in an elastic half-space with the goal of identifying the relevant BCs that can provide the desired surface wave-control behavior.

Consider a homogeneous isotropic linear elastic half-space with the normal to the surface oriented in the $-x_3$ direction and wave propagation along x_1 direction (Fig. 1). Plane strain condition is assumed along x_2 direction to constrain the analysis to a two-dimensional case. The wave equation in the half-space is governed by Navier's second-order partial differential equation [35]

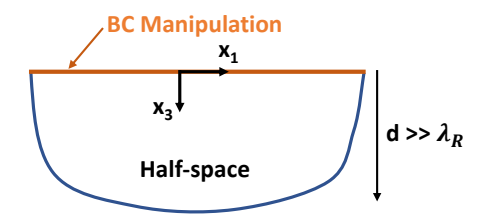


Figure 1: Schematic representation of an elastic half-space with different boundary conditions.

$$(\lambda + \mu)\nabla\nabla \cdot \bar{u} + \mu\nabla^2 \bar{u} = \rho \ddot{\bar{u}},\tag{1}$$

where λ and μ are Lamè material constants, ρ is the density, and $\bar{u}=(u_1,0,u_3)$ is the displacement vector under plane strain assumption. Using the Helmholtz decomposition of the displacement into scalar potential $\phi(x_1,x_3)$ and vector potential $\bar{\psi}=(0,\psi(x_1,x_3),0), \bar{u}=\nabla\phi+\nabla\times\bar{\psi}, \nabla\cdot\bar{\psi}=0$, leads to longitudinal and transverse bulk wave solutions [35, 36]

$$\nabla^2 \phi = \frac{1}{c_L^2} \frac{\partial^2 \phi}{\partial t^2},\tag{2}$$

$$\nabla^2 \psi = \frac{1}{c_T^2} \frac{\partial^2 \psi}{\partial t^2},\tag{3}$$

where c_L and c_T are the longitudinal and transverse bulk wave speeds, respectively. Here, we assume harmonic wave solutions traveling with a phase speed of c in the x_1 direction with amplitude variation $(D_1(x_3))$ and $D_2(x_3)$ in the x_3 direction

$$\phi = D_1(x_3)e^{ik(x_1 - ct)},\tag{4}$$

$$\psi = D_2(x_3)e^{ik(x_1 - ct)},\tag{5}$$

where k is the wave number. Substituting the wave solutions into Eqs. (2) and (3) and seeking surface wave solutions that decay in the x_3 direction, we obtain

$$\phi = A_1 e^{-kqx_3} e^{ik(x_1 - ct)},\tag{6}$$

$$\psi = B_1 e^{-ksx_3} e^{ik(x_1 - ct)}. \tag{7}$$

Thus, the displacement components are

$$u_1 = \frac{\partial \phi}{\partial x_1} - \frac{\partial \psi}{\partial x_3} = k(iA_1e^{-kqx_3} + sB_1e^{-ksx_3})e^{ik(x_1 - ct)}, \tag{8}$$

$$u_3 = \frac{\partial \phi}{\partial x_3} + \frac{\partial \psi}{\partial x_1} = k(-qA_1e^{-kqx_3} + iB_1e^{-ksx_3})e^{ik(x_1 - ct)}, \tag{9}$$

while Hooke's law gives the stress components

$$\sigma_{33} = \lambda \left(\frac{\partial u_1}{\partial x_1} \right) + (\lambda + 2\mu) \left(\frac{\partial u_3}{\partial x_3} \right)$$
$$= \mu k^2 (rA_1 e^{-kqx_3} - 2isB_1 e^{-ksx_3}) e^{ik(x_1 - ct)}, \quad (10)$$

$$\sigma_{13} = \mu \left(\frac{\partial u_3}{\partial x_1} + \frac{\partial u_1}{\partial x_3} \right)$$

$$= -\mu k^2 (2iqA_1 e^{-kqx_3} + rB_1 e^{-ksx_3}) e^{ik(x_1 - ct)}, \quad (11)$$

where $q=\sqrt{1-\frac{c^2}{c_L^2}}$, $s=\sqrt{1-\frac{c^2}{c_T^2}}$, and $r=2-\frac{c^2}{c_T^2}$. In these equations, σ is the Cauchy stress tensor. The constants A_1 and B_1 can be determined using the BC information on the top surface $(x_3=0)$ of the half-space.

Imposing the Neumann (traction-free) BCs ($\sigma_{33} = \sigma_{13} = 0$) on the surface of the half-space results in the well-known Rayleigh surface waves [37], whereas imposing the Dirichlet BCs ($u_1 = u_3 = 0$) results in nondispersive surface waves [35] that propagate with a phase speed of $c = \sqrt{c_T^2 + c_L^2}$. Next, let us evaluate

the possible surface wave solutions for the following Cauchy type BCs that are of interest to this study:

• Mindlin BCs, a representation of a lubricated rigid surface, are Cauchy type BCs that constrains the traction component in the x_1 direction and the displacement component in the x_3 direction on the surface of the elastic half-space:

$$\sigma_{13} = u_3 = 0, \quad for \quad x_3 = 0.$$
 (12)

This BC was initially proposed by Mindlin [38] to decouple the longitudinal (L) and shear vertical (SV) wave modes in isotropic plates and was later extended by Solie and Auld for anisotropic plates [39]. Though this BC application was initially considered unrealistic [39], recently, Lissenden et al. have shown a promising application of this BC to suppress the low-frequency Lamb wave A0 mode in a frequency-dependent manner using rod-like resonators on the surface of an isotropic plate [30]. Interestingly, solving Eqs. (9) and (11) by imposing the Mindlin BCs (Eq. (12)) results in only a trivial solution to the eigenvalue problem suggesting no surface wave propagation. In other words, Mindlin BCs seem to provide the desired control by forbidding the propagation of Rayleigh waves.

• Auld BCs, a taut-chain representation of the surface, is another Cauchy type BC, which constrains the traction component in the x_3 direction and the displacement component in the x_1 direction on the surface of the elastic half-space:

$$\sigma_{33} = u_1 = 0, \quad for \ x_3 = 0.$$
 (13)

Similar to Mindlin BC, Auld BC was also proposed by Mindlin and later extended by Solie and Auld to decouple wave modes. These BCs were recently exploited to reflect the low-frequency Lamb wave S0 mode in an isotropic plate at a prescribed frequency using clamping resonators

[32, 30]. Solving Eqs. (8) and (10) together with imposing the Auld BCs (Eq. (13)) results in a non-dispersive shear vertical wave propagation in the x_1 direction having no x_3 amplitude dependence with the following displacement solutions:

$$u_1 = 0, (14)$$

$$u_3 = iAe^{ik(x_1 - c_T t)}. (15)$$

Based on this analysis, Mindlin BCs show promise for preventing the propagation of Rayleigh waves. Though the analytical derivation provides insight into the influence of Mindlin BCs on the surface wave propagation, it is simplified and requires validation through detailed numerical investigations.

3. NUMERICAL ANALYSIS

We use numerical simulations to further investigate how Mindlin BCs applied over a finite region of the surface influence Rayleigh wave propagation in an elastic half-space. Frequency domain and time domain finite element simulations are conducted to study the nature of mode-converted wave modes and the minimum required length for the region with modified BCs (Mindlin BCs). Such an analysis is necessary for designing resonators to impose Mindlin BCs, an example of which is shown in in Section 5.

is 3.1. FREQUENCY DOMAIN ANALYSIS

To investigate the interaction of Rayleigh waves with the imposed Mindlin BCs on the surface, a 3D frequency-domain finite element (FDFE) study is performed using COMSOL Multiphysics® software (version 5.6) [40]. However, the simulations provide planar solutions due to the imposed periodic BCs in $\pm x_2$ directions. An elastic half-space is modeled with thickness $16\lambda_R$ in the x_3 direction (Fig. 2) and material properties of Aluminium (Density of 2700)

Kg/m³, Young's modulus of 69 GPa and Poisson ratio of 0.33). As shown in Fig. 2, the half-space is partitioned along its length into multiple domains: "buffer" region of length $1\lambda_R$, "excitation" region of length $10\lambda_R$, "incident" region of length $\alpha\lambda_R$, and "Mindlin BC" region of length $\beta\lambda_R$, where λ_R is the wavelength of the Rayleigh wave, and α and β are two positive constants. A perfectly matched layer (PML) of thickness $2\lambda_R$ is considered on all the boundaries except the top surface to prevent the "end-wall" reflection. A body load excitation with stresses corresponding to Rayleigh wave propagation is applied in the incident region to simulate incident Rayleigh waves.

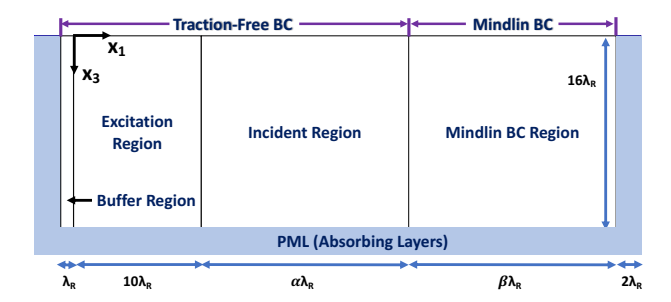


Figure 2: Schematic of the elastic half-space model having traction-free BCs in "Excitation" and "Incident" regions and imposed Mindlin BCs on the surface of the "Mindlin BC" region.

Traction-free BCs are assumed on the top surface of the model except the "Mindlin BC" region, where Mindlin BCs are imposed by constraining the displacement in x_3 direction. An element mesh size of 2.09 mm ($\sim \lambda_R/10$) and frequency (f) of 100 kHz ($\lambda_R = 29.09$ mm) are used for the numerical analysis. The simulated displacement fields for $\alpha = 16$ and $\beta = 16$ are shown in Fig. 3. The complex displacements in the x_1 and x_3 directions, obtained from COMSOL simulations, are denoted as U_1 and U_3 , respectively. The Re(U_1) and Re(U_3) displacement profiles confirm the expected surface wave control with no Rayleigh wave propagation visible in the "Mindlin BC" region (Fig. 3). However, wave mode conversions are apparent in both the "incident" and the "Mindlin BC" regions that require further investigation.

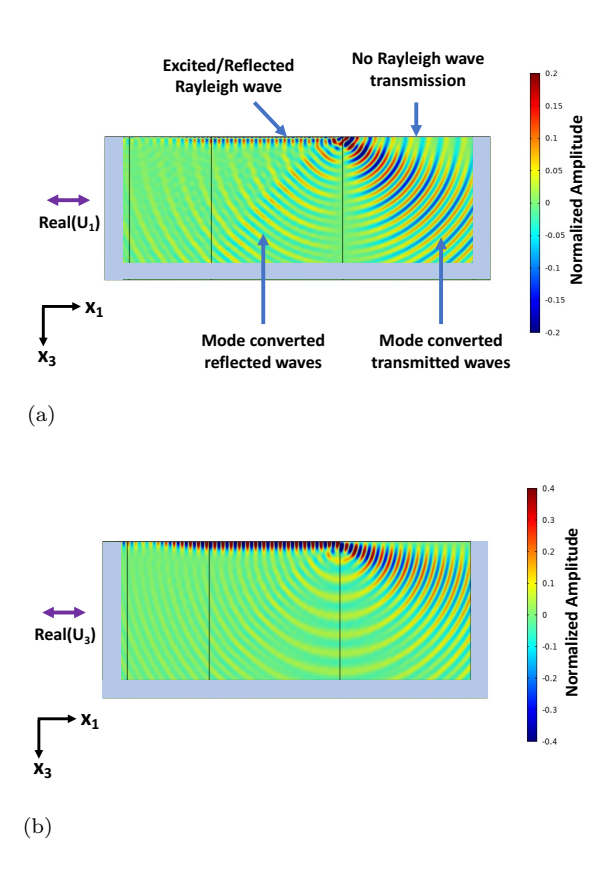


Figure 3: The displacement fields obtained by imposing Mindlin BCs on the surface of the "Mindlin BC" region: (a) $\operatorname{Re}(U_1)$, (b) $\operatorname{Re}(U_3)$. U_1 and U_3 are the complex displacement data in the x_1 and x_3 directions normalized with respect to the magnitude of total real displacement.

We use the short spatial Fourier transform (SSFT) to identify the mode-converted waves. The spatial Fourier transform (SFT) is a powerful tool to distinguish different reflected and transmitted wave modes in FDFE analysis [41]. The SFT of the simulated complex displacement profile "recorded" along an edge ("data line") in the model gives the wavenumber spectrum. In case of plane-wave propagation, the SFT wavenumber spectrum would have distinct peaks that correspond to particular wave modes. However, SFT of a "data line" in the path of circular-crested waves may result in overlapping peaks in the wavenumber spectrum thus complicating the identification of a particu-

lar wave mode. It is evident from Fig. 3 that the mode-converted reflected and transmitted waves originate from a point source at the intersection of the traction-free and Mindlin BCs and propagate at an oblique angle with a significant amount of radial spreading, making SFT unsuitable. Therefore, we adopt a SSFT for the analysis instead. The SSFT consists of applying SFT to a small range of data points around the point of interest to provide a local estimate of the wavenumber values. To obtain the desired wavenumber resolution, SSFT should be applied over a sufficient number of data points around the point of interest, which may require an increased model size.

To identify the mode-converted wave modes in Fig. 3 with a sufficiently fine wavenumber resolution, we create two additional models (case #1 and case #2), similar to the one used in Fig. 3 but larger, with a thickness of $24\lambda_R$. In case #1, we set $\alpha = 4$ and $\beta = 24$ to enlarge the "Mindlin BC" region and study the nature of transmitted mode-converted waves as illustrated in Fig. 4(a). Whereas case #2 is modeled with $\alpha = 24$ and $\beta = 4$ to study the reflected mode-converted waves in the enlarged "incident" region show in Fig. 5(a). The complex displacement data (U_1 and U_3) is extracted along three horizontal and vertical "data lines" separated by a distance of $2\lambda_R$ at the center of the "Mindlin BC" region for case #1 and the "incident" region for case #2, respectively (see Figs. 4(a) and 5(a)) for the wavenumber spectra analysis. SSFT is then applied to the complex displacement components (U_1 and U_3) obtained over 7500 data points within a length of $8\lambda_R$ around each of the nine intersection points marked in Fig. 4(a) to obtain the local wavenumber spectra. An illustrative example of the data points used to construct the wavenumber spectra for the intersection point at the center of the "Mindlin BC" region is shown in the insets of Figs. 4(b) and 4(c). The SSFT of the displacement profiles along the horizontal and vertical lines provides wavenumber projections in x_1 (k_x) and x_3 (k_z) directions, respectively. The corresponding k_x and k_z wavenumber spectra for the intersection point at the center of the grid are shown in Figs. 4(b) and 4(c). The resultant wavenumber $k = \sqrt{(k_x^2 + k_z^2)}$ and its corresponding wave speed provides information about the wave modes propagating through the intersec-

tion point. A similar analysis is performed for case #2 but in the "incident" region to study the mode-converted reflected waves, as illustrated in Fig. 5. Note that all the presented wavenumber spectra in Figs 4 and 5 are normalized with respect to the spectral amplitude corresponding to the incident Rayleigh wave calculated by SSFT of $U_1 + U_3$ extracted along a $8\lambda_R$ long line (7500 data points) on the surface at the center of the "incident" region.

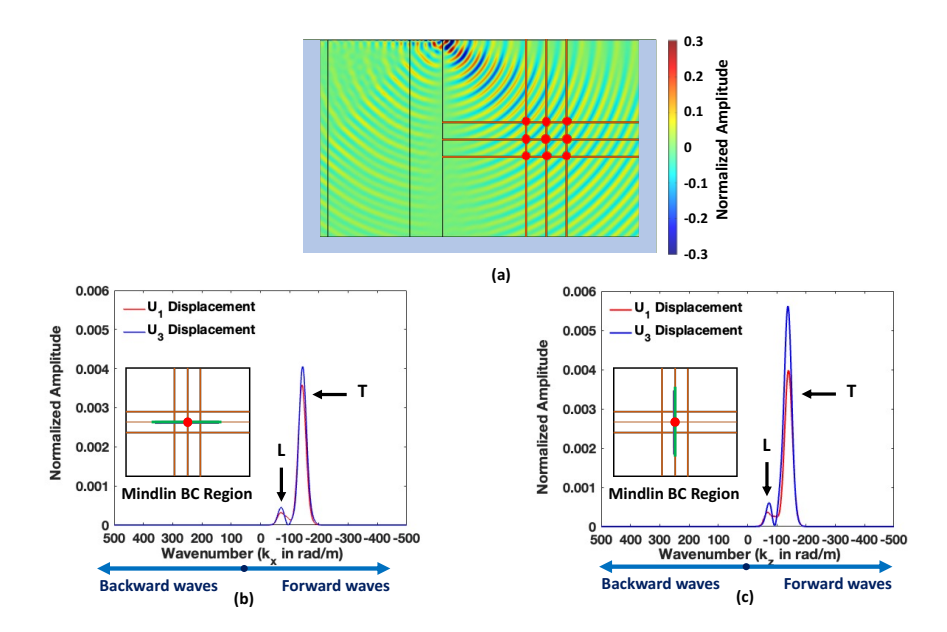


Figure 4: COMSOL FDFE simulation results for case #1: (a) the $Re(U_1)$ surface displacement profile and the data lines used for SSFT analysis. The normalized wavenumber spectra (k_x) and k_z obtained through SSFT analysis in the (b) x_1 direction and (c) x_3 direction are presented for the intersection point located at the center of the "Mindlin BC" region (marked in red). The insets in (b) and (c) provide schematics of the data points (marked in green) used for the SSFT. The peaks corresponding to longitudinal (L) and transverse (T) waves are marked for reference.

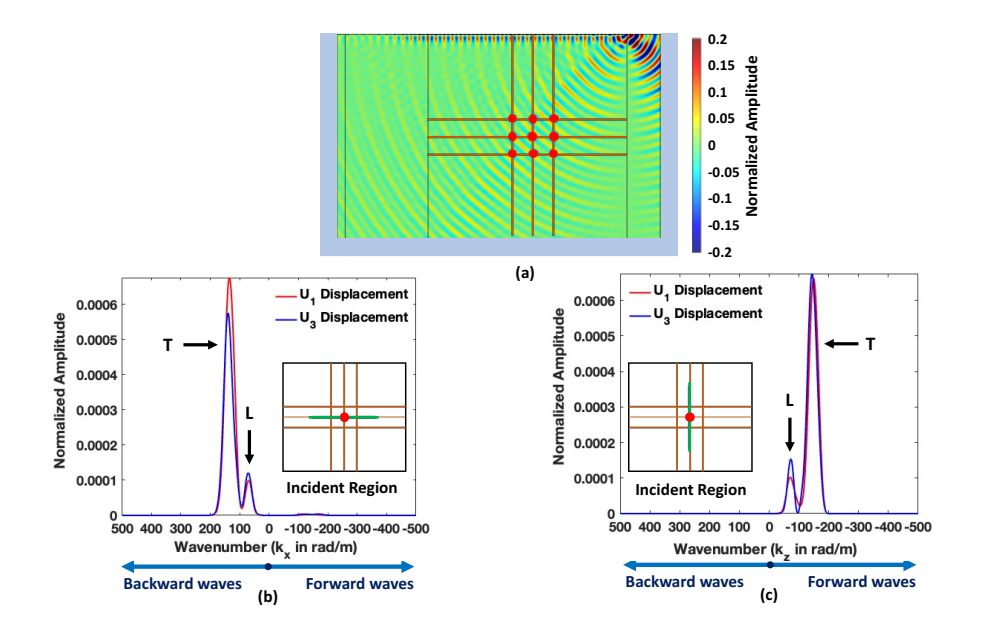


Figure 5: COMSOL FDFE simulation results for case #2: (a) the $Re(U_1)$ surface displacement profile and the data lines used for SSFT analysis. The normalized wavenumber spectra (k_x and k_z) obtained through SSFT analysis in the (b) x_1 direction and (c) x_3 direction are presented for the intersection point located at the center of the "Mindlin BC" region (marked in red). The insets in (b) and (c) provide schematics of the data points (marked in green) used for the SSFT. The peaks corresponding to longitudinal (L) and transverse (T) waves are marked for reference.

To interpret the wavenumber spectra shown in Figs. 4 and 5, we should note that the solid mechanics module of COMSOL assumes harmonic solutions of the form $e^{i\omega t}$ to the wave problem in frequency domain analysis, where ω is the angular frequency, and t is time. Therefore, as marked on the spectra, the positive and negative wavenumbers indicate the backward and forward wave propagation, respectively. The k_x and k_z wavenumber spectra for both cases indicate two distinct peaks. For case #1, the average wavenumbers estimated from the displacements U_1 and U_3 around the center intersection point are k_x = -70 rad/m and k_z = -137.8 rad/m for the larger second peak (Fig. 4). This gives estimated

wavenumbers k = -99.5 rad/m and -199.5 rad/m for the first and second peaks, respectively. These wavenumbers can be converted to phase speeds using the expression $c = 2\pi f/k$, resulting in values (c = 6311.2 m/s and 3147.8 m/s) corresponding closely to the expected wave speeds of longitudinal ($c_L = 6197$ m/s) and transverse ($c_T = 3122 \text{ m/s}$) waves. This analysis is repeated for all the nine intersection points and the range of calculated wave speeds corresponding to both peaks is plotted in Fig. 6(a). The aggregated wave speeds strongly indicate the presence of mode-converted longitudinal and transverse waves in the "Mindlin BC" region. A similar procedure is followed to identify the wave modes in the wavenumber spectra corresponding to case #2 shown in Figs. 5(b) and 5(c). The aggregated wave speeds (for all nine intersection points) corresponding to the two peaks in case #2 are plotted in Fig. 6(b). Similar to the transmitted waves, we observe the presence of reflected longitudinal and transverse waves in the incident region following the Rayleigh wave-Mindlin BC interaction. This analysis indicates that Rayleigh waves incident upon Mindlin BCs convert into bulk waves.

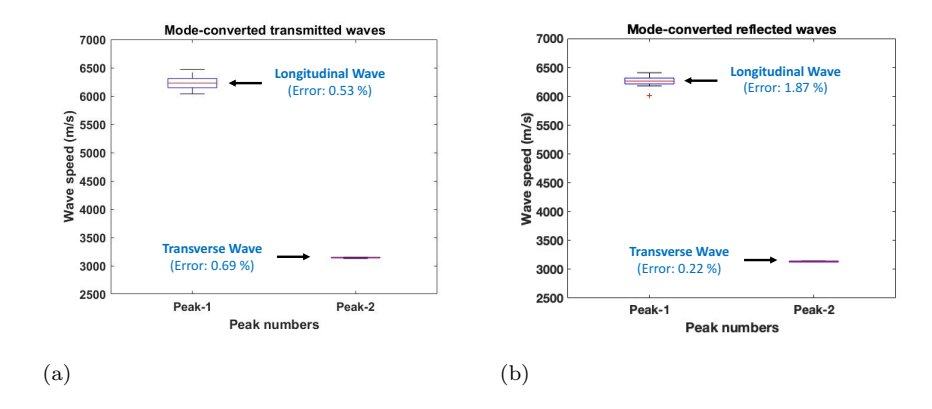


Figure 6: The calculated wave speeds corresponding to mode-converted (a) transmitted and (b) reflected waves obtained through SSFT of the displacement profiles around the nine intersection points. The box plot graphically represents the minimum, first quartile, median, third quartile, and maximum of the aggregated data.

To study the reflected and transmitted waves along the surface, SSFT is used to obtain wavenumber (k_x) spectra for surface displacement at the center of the

"incident" region of case #2 and the "Mindlin BC" region of case #1. The resulting k_x spectra are shown in Fig. 7. The incident/reflected wavenumber spectrum indicates a low amplitude reflected Rayleigh wave upon incidence on the Mindlin BC region (Fig. 7(a)). The larger peaks at the wavenumber k =-215.9 rad/m in Fig. 7(a) correspond to the incident Rayleigh wave. The peaks corresponding to reflected longitudinal and transverse waves are not visible in Fig. 7(a) as the amplitudes of these wave modes on the surface are insignificant compared to the reflected Rayleigh wave. As expected, the wavenumber spectrum of the surface displacement in the transmitted region displays two peaks corresponding to the longitudinal and transverse waves with no Rayleigh wave transmission (Fig. 7(b)). Note that the transmitted longitudinal and transverse wave amplitudes are very small near the surface, as evident from their normalized amplitudes in Fig. 7(b). It is also interesting to observe that the mode-converted longitudinal waves have a larger amplitude than transverse waves near the surface (Fig. 7(b)), in contrast to what is observed earlier within the "Mindlin BC" region (Figs. 4(b) and 4(c)). The relatively smaller amplitude of transverse waves could be attributed to the constraint on the vertical displacement (u_3) along the surface of the "Mindlin BC" region.

The above-described FDFE analyses confirm our analytical findings that applying Mindlin BCs on the surface forbids Rayleigh wave propagation. To provide further evidence for Rayleigh to bulk wave mode conversion and the efficacy of Mindlin BCs for suppressing surface waves, time domain studies are performed, as described in the subsequent section.

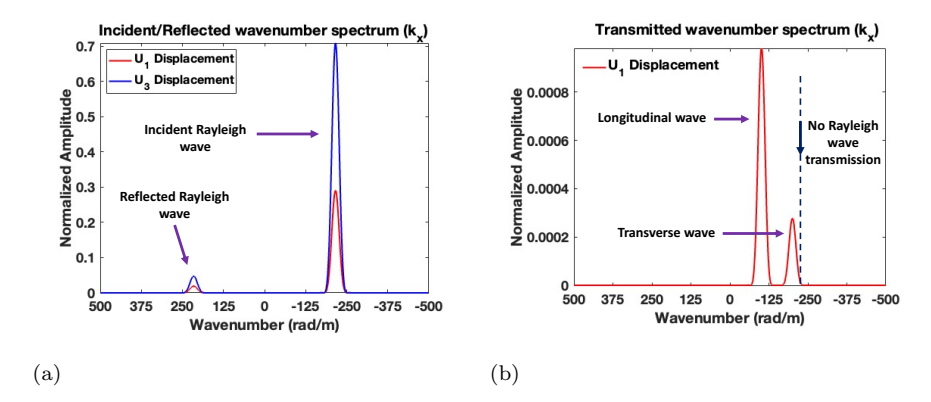


Figure 7: Wavenumber spectra for surface displacement: (a) incident/reflected wavenumber spectra corresponding to the surface displacement of the "incident" region in case #2 and (b) transmitted wavenumber spectrum corresponding to the surface displacement of the "Mindlin BC" region of case #1.

3.2. TIME DOMAIN ANALYSIS

A 2D model is considered for the time-domain finite element (TDFE) simulations performed in ABAQUS FEA software (Version 2018) [42], with multiple regions similar to those used for FDFE studies (Fig. 2). The model parameters determining the extent of "incident" and "Mindlin BC" regions, α and β , are both set to 15. A 30 mm ($\sim \lambda_R$) thick layer of "infinite elements" is used as an absorbing layer on the outer boundaries of the model to prevent "end-wall" reflections. The material (aluminum) properties are identical to those used in FDFE models. Many studies suggest using point load or wedge excitation to simulate Rayleigh waves [43, 23]. However, both of these methods have their inherent disadvantages; the former resulting also in bulk wave excitation and the latter resulting in undesired reflections and mode-conversions within the wedge. Here, we use a line-load excitation by applying the Rayleigh wave structure (displacement profile) along the edge of the excitation region, as shown in Fig. 8(d). A 5-cycle Hanning windowed harmonic pulse of f = 100 kHz central frequency with a bandwidth of 85 kHz to 115 kHz at -6 dB is defined (Figs. 8(a) and 8(b)). Since the displacement components (u_1 and u_3) of Rayleigh waves are 90-degree out of phase, two out-of-phase pulses are input to the model along

the x_1 and x_3 directions, as illustrated in Fig. 8(c). A structured 4-node plane strain quadrilateral (CPE4R) mesh of size $\Delta x = 1$ mm ($\sim \lambda_R/30$) and a stable time increment of 50 ns (< 1/(20f) and $< \Delta x/20$) is used for the analysis. Infinite layers comprise 4-node linear plane strain infinite elements (CINPE4).

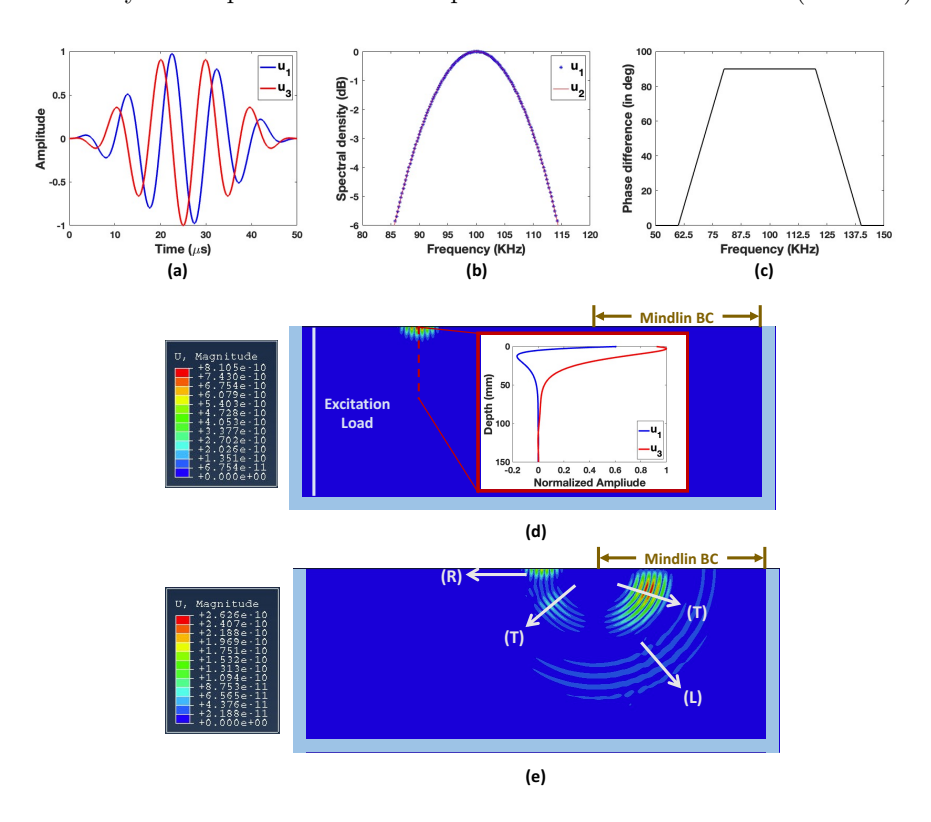


Figure 8: Time domain analysis excitation pulse and results: (a) two out-of-phase 5-cycle Hanning windowed harmonic pulses corresponding to u_1 and u_3 displacements and their corresponding (b) frequency spectrum and (c) phase difference. Two snapshots showing wave propagation (displacement magnitude) from the TDFE simulation at times (d) $129\mu s$ and (e) $345\mu s$ after sending the pulse. The displacement field in (d) shows pure Rayleigh wave propagation in "incident" region resulting from the line-load excitation (at the location marked with a white vertical line) with the inset illustrating the two displacement components (u_1 and u_3) of the propagating Rayleigh wave packet. The displacement field in (e) shows the reflected and transmitted mode-converted longitudinal (L) and transverse (T) waves as well as reflected Rayleigh (R) wave after encountering Mindlin BCs.

The simulation results at two time instances $129\mu s$ and $345\mu s$, before and after the Rayleigh wave interaction with Mindlin BCs, are shown in Figs. 8(d) and 8(e), respectively. Fig. 8(d) shows the efficacy of the line-load excitation model to excite only the Rayleigh wave; the displacement profiles $(u_1 \text{ and } u_3)$ in the inset corresponding to the depicted wave packet confirm pure Rayleigh wave propagation. The displacement field at time $345~\mu s$ (Fig. 8(e))agrees well with the frequency-domain analysis results and visually confirms the presence of mode-converted reflected and transmitted bulk waves and Rayleigh wave reflection upon the interaction of the incident Rayleigh wave with the Mindlin BCs. For a more quantitative analysis of the reflections/mode conversions, a two-dimensional Fourier analysis is performed to obtain the dispersion characteristics (k-f) spectrum of the mode-converted waves. The results of the dispersion analysis are discussed in the supplementary material.

4. Effect of Mindlin BC patch length on the Rayleigh wave propagation

Having established the efficacy of Mindlin BCs in forbidding surface wave propagation, a parametric analysis is performed to examine the influence of the "Mindlin BC" region length ("patch length") on the Rayleigh wave propagation. We investigate the practical question: what is the minimum Mindlin BC "patch length" required to suppress the Rayleigh wave propagation? To answer this question, a similar COMSOL model to that in Fig. 2 is created. But, the new model has an additional region with traction-free surface ("transmitted" region) of the same length as the "incident" region $(\alpha \lambda_R)$ added after the "Mindlin BC" region. The parameter α representative of the length of the incident and transmitted regions is set to 15. To vary the Mindlin BC "patch length", the parameter β is varied as 1, 2, 5, 10, and 15. A FDFE simulation at 100 kHz is conducted using each of the models with a different Mindlin BC "path length" corresponding to the different β values.

The displacement $(Re(U_3))$ fields for the different patch langths, β values

of 1, 2, 5, 10, and 15, are shown in Figs. 9(a) through 9(e), respectively. The simulation results show that the mode conversion happens right at the interface between the "incident" and "Mindlin BC" regions, similar to the A0 Lamb wave mode conversions demonstrated in [30]. However, the transmitted bulk waves near the surface undergo a mode conversion back to Rayleigh waves at the interface between the "Mindlin BC" and the "transmitted" regions. As the Mindlin BC "patch length" increases in Figs. 9(c) through 9(e), the bulk waves travel sufficiently far into the bulk of the transmitted region, reducing the extent of mode-conversion back to Rayleigh waves.

Fig. 9(f)-(i) shows the wavenumber spectra for the surface displacement in the incident/reflected (Figs. 9(f) and 9(g)) and transmitted regions (Figs. 9(h) and 9(i)). To calculate the wavenumber spectra, SSFT is applied to complexvalued surface displacement data corresponding to 7500 points spanning over $8\lambda_R$ in the middle of the "incident" and "transmitted" region surfaces. The wavenumber spectra are normalized with respect to the spectral amplitude of the incident Rayleigh wave at 100 kHz obtained by SSFT of the complex-valued surface displacement data $(U_1 + U_3)$ in "incident" region (7500 data points). The incident/reflected wavenumber spectra indicate a Rayleigh wave reflection with an amplitude, which is about 7% of the incident wave amplitude (Fig. 9(f) and 9(g)). Moreover, the amplitude of reflected Rayleigh wave is observed to be independent of the Mindlin BC patch length. This is expected as the reflection occurs at the interface between the incident and Mindlin BC regions and thus is independent of the extent of the Mindlin BC patch. In contrast, Rayleigh wave transmission significantly decreases as the Mindlin BC "patch length" increases from $1\lambda_R$ to $15\lambda_R$ (Figs. 9(h) and 9(i)). While the $1\lambda_R$ long Mindlin BC patch provides a 74% reduction in Rayleigh wave transmission, 99% transmission reduction is achieved for Mindlin BC "patch lengths" of more than $10\lambda_R$ (Figs. 9(h) and 9(i)). These observations agree with our previous understanding that the second mode conversion (mode-converted bulk waves to Rayleigh waves) is solely due to the proximity of the transmitted bulk waves to the next traction-free surface in the transmitted region. As the reflected Rayleigh wave is independent of the patch length, the amount of Rayleigh wave suppression achieved quantitatively represents the extent of mode-conversion of Rayleigh waves to bulk waves. In addition, a low-amplitude wavenumber peak corresponding to the longitudinal wave is observed in the transmitted wavenumber spectra visible only in the insets of Figs. 9(h) and 9(i). However, there is no evidence of transmitted transverse waves near the surface in the transmitted wavenumber spectra. This could be a consequence of the second mode conversion from transverse to Rayleigh wave, which eliminates transverse wave propagation near the surface.

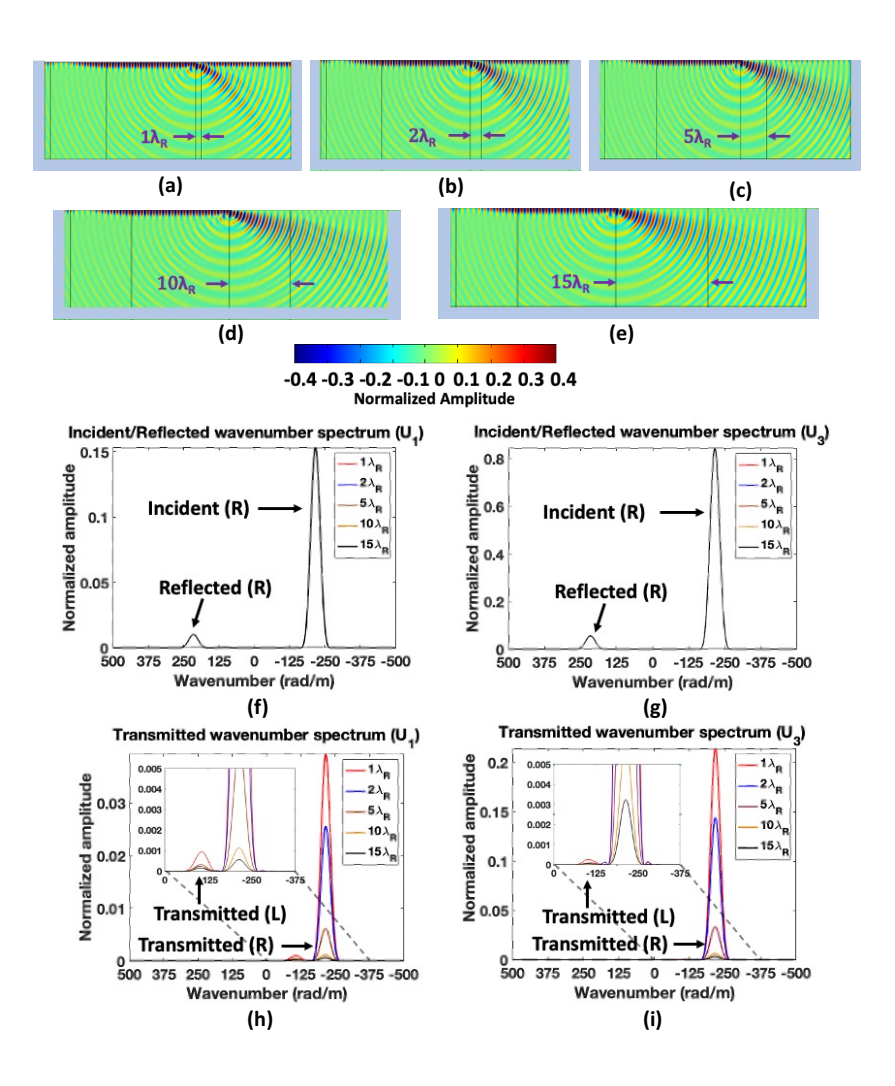


Figure 9: COMSOL FDFE simulation results for varying Mindlin BC patch lengths: the displacement field (Re(U_3)) across the model normalized with respect to the maximum value of the total real displacement for the Mindlin BC "patch length" of: (a) $1\lambda_R$ (b) $2\lambda_R$, (c) $5\lambda_R$, (d) $10\lambda_R$, and (e) $15\lambda_R$. The incident/reflected wavenumber spectra correspond to (f) U_1 and (g) U_3 obtained on the surface of "incident" region. The transmitted wavenumber spectra correspond to (h) U_1 and (i) U_3 on the surface of "transmitted" region. The legend indicates the Mindlin BC "patch length" in terms of Rayleigh wavelength λ_R . The longitudinal (L), transverse (T), and Rayleigh (R) waves are marked for reference. The insets in subfigures (h) and (i) provide the enlarged view of the peaks corresponding to the transmitted longitudinal waves. The wavenumber spectra in subfigures (f) - (i) are normalized with respect to the spectral amplitude corresponding to the peak of the incident Rayleigh wave.

The mode conversions are further investigated using an ABAQUS TDFE simulation (Section 3.2) with a $5\lambda_R$ long Mindlin BC patch. The first mode conversion is clearly visible in Fig. 10(b), resulting in mode converted bulk waves and Rayleigh wave reflection. The conversion happens immediately after Rayleigh wave impinges upon the interface between the "incident" region and Mindlin BC path similar to that observed for mode-conversions of low-frequency Lamb waves [30]. The snapshots of the wave propagation illustrating the second mode conversions are presented in Fig. 10(c) and 10(d). Fig.10(c) shows the mode conversion from the transverse wave to the Rayleigh wave at the end of the "Mindlin BC" region. The parametric study presented earlier suggests a minimum "patch length" of $10\lambda_R$ to prevent the second mode conversion and to sufficiently reduce Rayleigh wave transmission. These results are different from the recently achieved control of low-frequency Lamb waves, where a patch as small as $\lambda/100$ has shown to significantly reduce the transmitted waves [30].

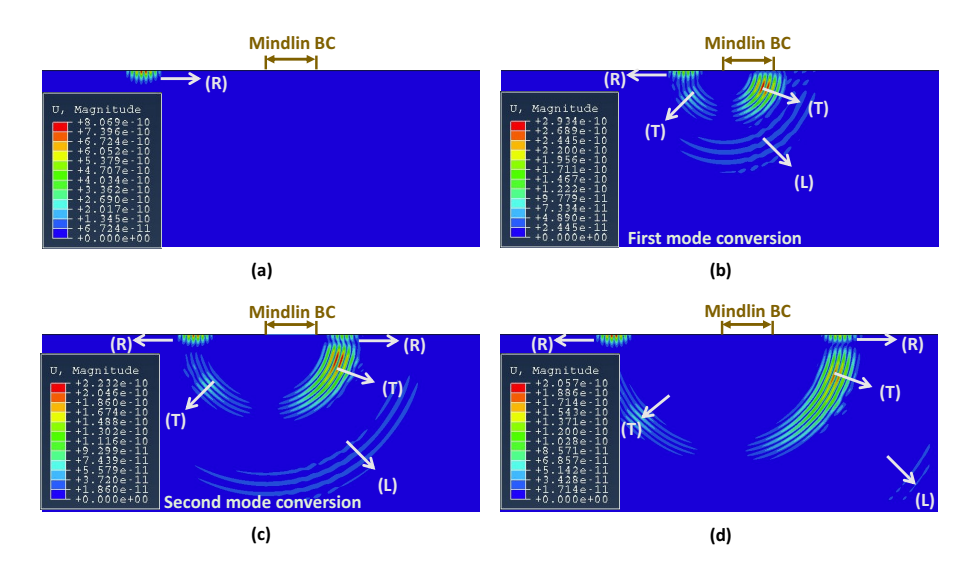


Figure 10: Snapshots of the displacement field from the TDFE simulations of Rayleigh wave propagation in a half-space with a Mindlin BC patch of length $5\lambda_R$ at times (a) $102\mu s$, (b) $276\mu s$, (c) $309\mu s$ and (d) $351\mu s$ after sending the pulse. The longitudinal (L), transverse (T), and Rayleigh (R) waves are marked for reference.

5. Discussion

The TDFE simulation results show the asymmetry of the transmitted and reflected mode-converted bulk waves originating from the interface between the traction-free and Mindlin BC regions. Fig. 11 depicts the normalized displacement magnitude of the transverse and longitudinal waves in Fig. 8(e) captured at a propagation distance of 360 mm ($\sim 12\lambda_R$). Transverse waves exhibit two main amplitude lobes; the transmitted wave into the "Mindlin" BC region shows a maximum value at an angle θ of about 20 deg while the reflected wave into the "incident" region is maximum at $\theta = 135$ deg as marked in Fig. 11. As already discussed, it is clear from Fig. 11 that the dependence on the patch length for the second mode conversion is due to the closeness of the amplitude lobe corresponding to the transmitted transverse wave (20 deg) to the traction-free surface of the "transmitted" region. The mode-converted longitudinal wave is observed to have maximum amplitude at 60 deg into the "Mindlin BC" region with a part of its wavefront in the "incident" region. Moreover, it is evident from Fig. 11 that the incident Rayleigh wave energy is predominantly transmitted as transverse bulk waves with minimal conversion to longitudinal and reflected transverse waves. In other words, the longitudinal wave amplitude is significantly smaller compared to the transverse waves. Slight distortions observed in the amplitude lobe corresponding to the longitudinal wave are likely due to the unsuppressed wave reflections from the model boundaries. Finally, a fictitious transverse wave lobe of high amplitude in the "incident" region near to the surface is due to the proximity of reflected Rayleigh and mode-converted transverse waves because of the closeness of their wave speeds and therefore, should be ignored. Besides, the Rayleigh wave reflection influences the amplitude profile of the lobe corresponding to the reflected transverse wave, resulting in a slight distortion of the amplitude lobe at angles greater than 150 deg. It is clear from Fig. 11 that the transmitted angles of the mode-converted transverse and longitudinal waves do not follow the Snell's law, $\cos \theta = (c_T/c_R)$, which is undefined. Future studies will include a careful study of Rayleigh reflection and refraction

due to the imposed BCs to better understand the reported observations here.

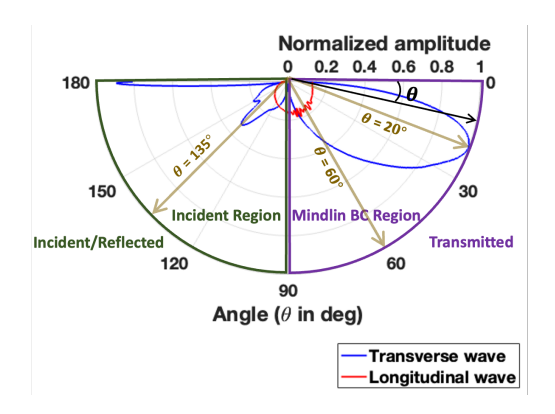


Figure 11: Polar plot representing the magnitude of the mode-converted longitudinal and transverse wave displacements in the "incident" and "Mindlin BC" regions. The wave propagation angles corresponding to the mode-converted longitudinal and transverse waves are marked for reference.

The above analyses suggests that imposing Mindlin BCs is effective in reflecting and mode converting the incident Rayleigh waves. Here, we demonstrate how to impose such BCs using a surface-mounted resonator. We hypothesize that a properly designed resonator on a half-space surface excited at its longitudinal resonance frequency may impose Mindlin BCs as in [30] and therefore, convert the incident Rayleigh wave into bulk waves according to our simulation results. To demonstrate the imposing of Mindlin BCs by a resonator around its resonance frequency, a 3D FDFE study is performed on a model that includes a single resonator mounted on an elastic half-space. Consistent with our previously shown FDFE studies, a 3D model of width 1 mm and thickness $6\lambda_R$ is partitioned into "buffer" region of length λ_R , "incident" and "transmitted" regions of length $4\lambda_R$, and a "resonator" region of length equal to the width of the resonator, as illustrated in Fig. 12(a). A prismatic rod-like resonator of length (L) 2.5 mm and 0.5 mm \times 0.5 mm cross-section (W×W) is mounted on the "resonator" region. The resonator size is chosen such that its first longitudinal resonance frequency is about 500 kHz (510 kHz) for fixed-free BCs, and the width (W) is decided to attain an aspect ratio (L/W) of 5. Periodic

BCs are imposed on the lateral boundaries of the half-space to ensure continuity in the displacement solutions. A line-load excitation with the displacement profiles corresponding to Rayleigh waves is applied over the left edge of the "incident" region and a frequency-domain study is performed at 490 kHz, 510 kHz (resonator's longitudinal resonance frequency, $\lambda_R = 5.4$ mm) and 530 kHz. A mesh of size of $\lambda_R/14$ is used for the numerical simulation. A similar model but with (frequency-independent) Mindlin BC patch in place of the resonator is also analyzed for comparison.

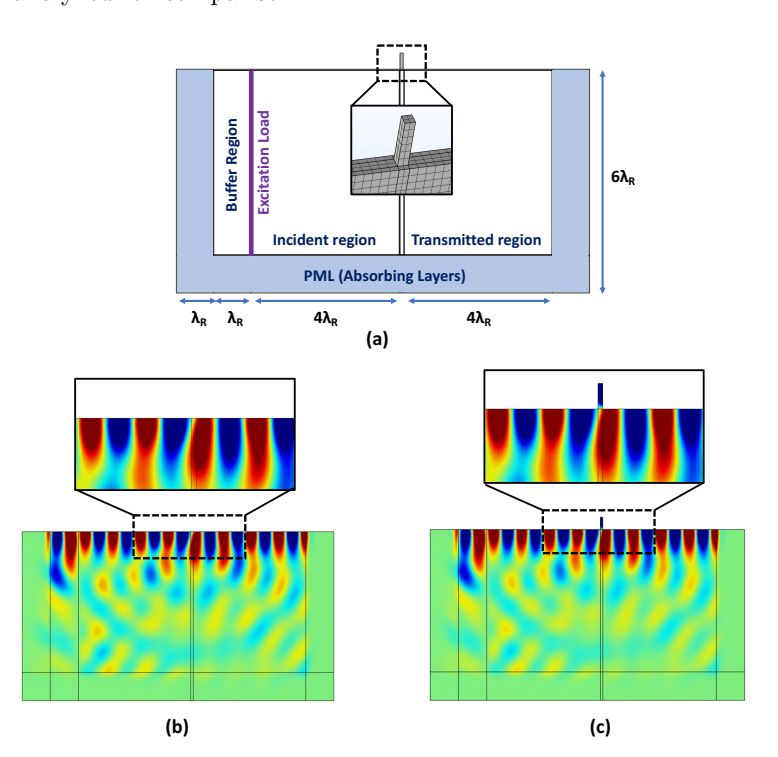


Figure 12: (a) Schematic of the elastic half-space model with a resonator and the displacement fields ($Re(U_3)$) obtained for the cases with (b) frequency-independent Mindlin BC patch and (c) a resonator with a first longitudinal resonance frequency at 510 kHz. The cut outs in subfigures (b) and (c) provide an enlarged view of the resonator and the near-surface "incident" and "transmitted" regions.

The simulation results at 510 kHz for the two analyzed cases of Mindlin BC patch and a single resonator are shown in Figs. 12(b) and 12(c), respectively.

The displacement fields $(Re(U_3))$ for the two cases are similar, both showing only 30% suppression of Rayleigh waves observed in the "transmitted" regions (estimated from the wavenumber spectrum analysis on surfaces of the "incident" and "transmitted" regions, not shown here). The low level of Rayleigh wave suppression is expected because of the small patch length or resonator width $(\sim \lambda_R/10)$ used for the simulation. The main question is whether the resonators impose Mindlin BCs on the surface of the elastic half-space. To answer this question, we examine the out-of-surface displacement profiles across the base of the resonator at resonance (510 kHz) and a few non-resonance frequencies as shown in Fig. 13. Also plotted are the profiles corresponding to displacements along the x (abs (U_1)) and y (abs (U_2)) directions at the resonance frequency (510 kHz). The out-of-surface displacement $abs(U_3)$ is found to be significantly smaller compared to $abs(U_1)$ at the resonant frequency. Also, $abs(U_2)$ is nearly zero possibly due to the wave propagation in the x-direction. More importantly, $abs(U_3)$ at 510 kHz is clearly smaller than that at non-resonance frequencies. These displacement profiles indicate that the resonator base is imposing Mindlin BCs at 510 kHz, the longitudinal resonance frequency.

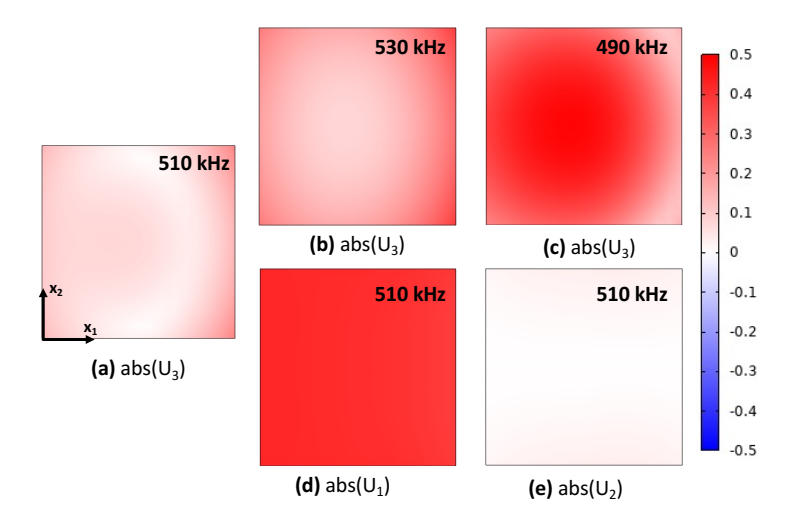


Figure 13: Surface displacement profiles at the base of the resonator: $abs(U_3)$ at (a) 510 kHz, (b) 530kHz, and (c) 490 kHz, and (d) $abs(U_1)$ and (e) $abs(U_2)$ at 510 kHz

Though the physics behind Rayleigh wave interaction with the prismatic rods (considering only the longitudinal motion of resonators) is demonstrated analytically in [23] by solving the boundary value problem, the explanation to the mode-conversion of Rayleigh wave to shear waves is not explicitly detailed. This analysis provides an insight into the mechanism that leads to the conversion of Rayleigh waves to the bulk waves using prismatic resonators. When using resonators to realize Mindlin BCs about the resonators' longitudinal resonance frequencies (Fig. 13(c)), it is impractical to achieve a patch length more than a Rayleigh wavelength. Therefore, because of the second mode conversion, it is impossible to achieve significant Rayleigh wave suppression using just a single resonator. However, the instantaneous first-mode conversion can be exploited to design an array of resonators mounted on sub-wavelength size patches to suppress the Rayleigh wave transmission successively. This is equivalent to an array of sub-wavelength-sized Mindlin BC patches, with each patch reflecting and converting the transmitted Rayleigh waves. As the Rayleigh wave propagates further through the array, it will lose more energy and will be diverted more and more away from the surface.

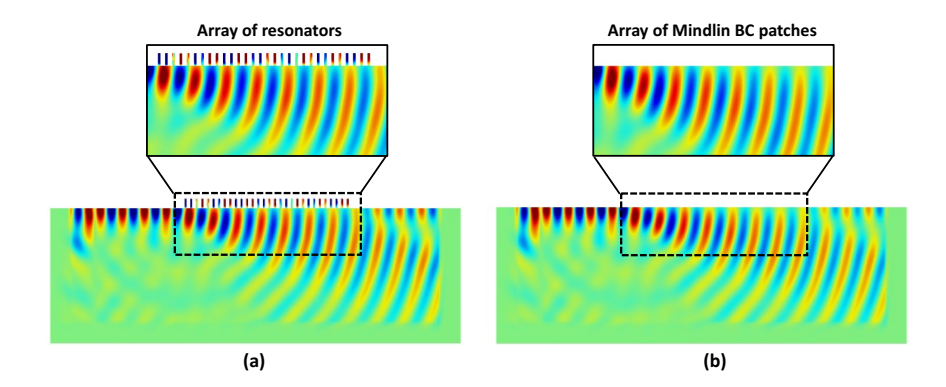


Figure 14: (a) Displacement fields $(Re(U_3))$ obtained for the cases with (b) an array of 30 resonators, each having their first longitudinal resonance frequency at 510 kHz and (c) an array of frequency-independent Mindlin BC patches. The cut outs in subfigures (a) and (b) provide an enlarged view of the resonator and the near-surface "incident" and "transmitted" regions.

The FDFE analysis performed on a single resonator (Fig. 12(a)) can be extended to an array of 30 resonators to confirm the imposing of Mindlin BCs by all the resonators at the longitudinal resonance frequency. To demonstrate this, we compare the displacement fields resulting from the interaction of the Rayleigh wave with an array of resonators (Fig. 14 (a)) and an array of an equal number of (frequency-independent) Mindlin BC patches (Fig. 14 (b)) at 510 kHz (longitudinal resonance frequency of the resonator). The dimensions of each Mindlin BC patch are identical to that of the resonator base and the spacing between the resonators/Mindlin BC patches is considered 1.4 mm ($\lambda_R/4$). The displacement fields ($Re(U_3)$) for both the cases (resonators/patches) are very similar, and show enhanced suppression of Rayleigh waves (90% suppression). These results indicate that an array of resonators impose an array of Mindlin BC patches (at 510 kHz) and thereby provide significant Rayleigh wave suppression. Many previous studies have reported the use of a surface-mounted resonator array to control Rayleigh wave propagation [28, 29, 7]. Although designing resonators based on longitudinal resonance frequency matching is straightforward, matching the BCs at the resonator base at prescribed frequencies could provide further insights into how the bandgaps are created leading to novel metasurface designs. However, the connection between imposing BCs and the generation of the bandgap is not yet fully explored. It should be noted that the closely spaced periodic resonators may lead to the incident Rayleigh wave dispersion, which can in turn influence the applied BCs responsible for the generated bandgap. Therefore, understanding the influence of Rayleigh wave dispersion on the BCs imposed by surface-mounted resonators is required for BC-based metasurface design and will be a part of future studies.

6. Conclusion

Understanding the interaction of surface waves with different boundary conditions can inspire novel metasurface designs similar to the recently established metasurface control over the low-frequency Lamb waves. An analytical study

using a particular Cauchy-type BC, called the Mindlin BC, shows promise for surface wave control, motivating the design of BC-based metasurfaces to manipulate Rayleigh wave propagation. The frequency-domain and time-domain finite element studies reveal the complexity of Rayleigh wave interaction with the Mindlin BCs, resulting in the reflection and transmission of the mode-converted longitudinal and transverse bulk waves. The presence of the mode-converted bulk waves is confirmed using an extensive wavenumber spectrum analysis that employs short spatial Fourier transforms. Two mode-converted transverse waves emanate from a point source at the intersection between the traction-free and BC regions. One is transmitted at about 20 degrees, and the other is reflected at 45 degrees from the top surface. The mode-converted longitudinal wave is observed to be transmitted at 60 degrees into the half-space. A Rayleigh wave reflection with an amplitude 1/15th of the incident wave is also observed in the simulation results. A parametric study reveals that the Mindlin BC region should be at least $10\lambda_R$ long to significantly block (99%) the Rayleigh wave propagation. A long patch is required because otherwise, the proximity of the transmitted bulk waves to the surface at the second interface (between Mindlin BC patch and traction-free 'transmission' regions) may result in a mode conversion from bulk waves back to Rayleigh waves. A surface-mounted resonator is shown to effectively impose Mindlin BCs at the resonator's longitudinal resonance frequency. However, using a single resonator may not provide significant Rayleigh wave suppression due to the constraint over the resonator geometry calling for a resonator array. Analogous to the clamping of the vertical displacement by a prismatic resonator, non-intuitive resonator designs are possible through topology optimization that imposes Mindlin BCs at desired frequencies. By further understanding and control over the transmitted bulk waves and considerations of attenuation and inhomogeneous granular half-space, this Mindlin BC-controlled metasurface design strategy can find applications in seismic isolation of structures and the design of surface acoustic wave devices, among others.

Acknowledgments

The authors gratefully acknowledge the support of the National Science Foundation under Grant No. 1934527. Any opinions, findings, and conclusions or recommendations expressed in this material are those of the author(s) and do not necessarily reflect the views of the National Science Foundation.

Computations for this research were performed on the Pennsylvania State
University's Institute for Computational and Data Sciences' Roar supercomputer.

References

- [1] F. E Richart, Vibrations of soils and foundations, Printed in the United States of America, 1970.
- [2] K. Länge, B. E. Rapp, M. Rapp, Surface acoustic wave biosensors: a review, Analytical and bioanalytical chemistry 391 (5) (2008) 1509–1519.
 - [3] C. Campbell, Surface acoustic wave devices and their signal processing applications, Elsevier, 2012.
- [4] C. Croënne, E. Manga, B. Morvan, A. Tinel, B. Dubus, J. Vasseur, A. C. Hladky-Hennion, Negative refraction of longitudinal waves in a two-dimensional solid-solid phononic crystal, Physical Review B 83 (5) (2011) 054301.
 - [5] R. Zhu, X. Liu, G. Hu, C. Sun, G. Huang, Negative refraction of elastic waves at the deep-subwavelength scale in a single-phase metamaterial, Nature communications 5 (1) (2014) 1–8.
 - [6] Y. Chen, J. Hu, G. Huang, A design of active elastic metamaterials for control of flexural waves using the transformation method, Journal of Intelligent Material Systems and Structures 27 (10) (2016) 1337–1347.
 - [7] A. Colombi, D. Colquitt, P. Roux, S. Guenneau, R. V. Craster, A seismic metamaterial: The resonant metawedge, Scientific reports 6 (1) (2016) 1–6.

- [8] S. S. Ramesh, M. C. Thippeswamy, P. Rajagopal, K. Balasubramaniam, Elastic metamaterial rod for mode filtering in ultrasonic applications, Electronics Letters 56 (19) (2020) 1024–1027.
- [9] M. Farhat, S. Guenneau, S. Enoch, Ultrabroadband elastic cloaking in thin plates, Physical review letters 103 (2) (2009) 024301.
 - [10] M. Farhat, S. Guenneau, S. Enoch, Broadband cloaking of bending waves via homogenization of multiply perforated radially symmetric and isotropic thin elastic plates, Physical Review B 85 (2) (2012) 020301.
- [11] A. N. Norris, A. L. Shuvalov, Elastic cloaking theory, Wave Motion 48 (6)
 (2011) 525–538.
 - [12] P. A. Deymier, Acoustic metamaterials and phononic crystals, Vol. 173, Springer Science & Business Media, 2013.
 - [13] Z. Liu, X. Zhang, Y. Mao, Y. Zhu, Z. Yang, C. T. Chan, P. Sheng, Locally resonant sonic materials, science 289 (5485) (2000) 1734–1736.
- [14] Y. Xiao, J. Wen, X. Wen, Flexural wave band gaps in locally resonant thin plates with periodically attached spring–mass resonators, Journal of Physics D: Applied Physics 45 (19) (2012) 195401.
 - [15] N. Fang, D. Xi, J. Xu, M. Ambati, W. Srituravanich, C. Sun, X. Zhang, Ultrasonic metamaterials with negative modulus, Nature materials 5 (6) (2006) 452–456.
 - [16] J. Y. Yoritomo, R. L. Weaver, P. Roux, M. Rupin, E. G. Williams, On band gap predictions for multiresonant metamaterials on plates, The Journal of the Acoustical Society of America 139 (3) (2016) 1282–1284.
- [17] E. G. Williams, P. Roux, M. Rupin, W. Kuperman, Theory of multiresonant metamaterials for a 0 lamb waves, Physical Review B 91 (10) (2015) 104307.

- [18] F. Meseguer, M. Holgado, D. Caballero, N. Benaches, J. Sanchez-Dehesa, C. López, J. Llinares, Rayleigh-wave attenuation by a semi-infinite twodimensional elastic-band-gap crystal, Physical Review B 59 (19) (1999) 12169.
- [19] S. Brûlé, E. Javelaud, S. Enoch, S. Guenneau, Experiments on seismic metamaterials: molding surface waves, Physical review letters 112 (13) (2014) 133901.
- [20] A. Khelif, Y. Achaoui, S. Benchabane, V. Laude, B. Aoubiza, Locally resonant surface acoustic wave band gaps in a two-dimensional phononic crystal of pillars on a surface, Physical Review B 81 (21) (2010) 214303.
 - [21] Y. Achaoui, A. Khelif, S. Benchabane, L. Robert, V. Laude, Experimental observation of locally-resonant and bragg band gaps for surface guided waves in a phononic crystal of pillars, Physical Review B 83 (10) (2011) 104201.
 - [22] A. Palermo, S. Krödel, K. H. Matlack, R. Zaccherini, V. K. Dertimanis, E. N. Chatzi, A. Marzani, C. Daraio, Hybridization of guided surface acoustic modes in unconsolidated granular media by a resonant metasurface, Physical Review Applied 9 (5) (2018) 054026.
- [23] D. Colquitt, A. Colombi, R. Craster, P. Roux, S. Guenneau, Seismic metasurfaces: Sub-wavelength resonators and rayleigh wave interaction, Journal of the Mechanics and Physics of Solids 99 (2017) 379–393.
 - [24] E. Garova, A. Maradudin, A. Mayer, Interaction of rayleigh waves with randomly distributed oscillators on the surface, Physical Review B 59 (20) (1999) 13291.
 - [25] A. Palermo, S. Krödel, A. Marzani, C. Daraio, Engineered metabarrier as shield from seismic surface waves, Scientific reports 6 (1) (2016) 1–10.

- [26] M. Miniaci, A. Krushynska, F. Bosia, N. M. Pugno, Large scale mechanical metamaterials as seismic shields, New Journal of Physics 18 (8) (2016) 083041.
- [27] N. Boechler, J. Eliason, A. Kumar, A. Maznev, K. Nelson, N. Fang, Interaction of a contact resonance of microspheres with surface acoustic waves, Physical review letters 111 (3) (2013) 036103.
- [28] A. Colombi, P. Roux, S. Guenneau, P. Gueguen, R. V. Craster, Forests as a natural seismic metamaterial: Rayleigh wave bandgaps induced by local resonances, Scientific reports 6 (1) (2016) 1–7.
 - [29] A. Colombi, V. Ageeva, R. J. Smith, A. Clare, R. Patel, M. Clark, D. Colquitt, P. Roux, S. Guenneau, R. V. Craster, Enhanced sensing and conversion of ultrasonic rayleigh waves by elastic metasurfaces, Scientific Reports 7 (1) (2017) 1–9.
 - [30] C. J. Lissenden, C. N. Hakoda, P. Shokouhi, Control of low-frequency lamb wave propagation in plates by boundary condition manipulation, Journal of Applied Physics 129 (9) (2021) 094903.
- [31] M. Rupin, F. Lemoult, G. Lerosey, P. Roux, Experimental demonstration of ordered and disordered multiresonant metamaterials for lamb waves, Physical review letters 112 (23) (2014) 234301.
 - [32] C. Hakoda, C. J. Lissenden, P. Shokouhi, Clamping resonators for low-frequency s0 lamb wave reflection, Applied Sciences 9 (2) (2019) 257.
- [33] Z. Cheng, Z. Shi, Novel composite periodic structures with attenuation zones, Engineering Structures 56 (2013) 1271–1282.
 - [34] Z. Shi, J. Huang, Feasibility of reducing three-dimensional wave energy by introducing periodic foundations, Soil Dynamics and Earthquake Engineering 50 (2013) 204–212.
 - [35] J. Achenbach, Wave propagation in elastic solids, Elsevier, 2012.

- [36] K. F. Graff, Wave motion in elastic solids, Courier Corporation, 2012.
 - [37] J. L. Rose, Ultrasonic guided waves in solid media, Cambridge university press, 2014.
 - [38] J. Yang, Introduction To The Mathematical Theory Of Vibrations Of Elastic Plates, An-By RD Mindlin, World Scientific, 2006.
- [39] L. Solie, B. Auld, Elastic waves in free anisotropic plates, The Journal of the Acoustical Society of America 54 (1) (1973) 50–65.
 - [40] COMSOL Multiphysics, User's manual version 5.6, COMSOL Inc.
 - [41] V. K. Chillara, B. Ren, C. J. Lissenden, Guided wave mode selection for inhomogeneous elastic waveguides using frequency domain finite element approach, Ultrasonics 67 (2016) 199–211.
 - [42] Abaqus/CAE User's Guide Version 6.13, User's manual version 5.6, Dassault Systèmes Simulia Corp.
- [43] M. Yuan, J. Zhang, S.-J. Song, H.-J. Kim, Numerical simulation of rayleigh wave interaction with surface closed cracks under external pressure, Wave
 Motion 57 (2015) 143–153.

Click here to access/download

LaTeX Source Files

elsarticle-num.bst

Click here to access/download **LaTeX Source Files**Figure 1.pdf

Click here to access/download **LaTeX Source Files**Figure 2.pdf

Click here to access/download **LaTeX Source Files**Figure3a.pdf

Click here to access/download **LaTeX Source Files**Figure3b.pdf

Click here to access/download **LaTeX Source Files**Figure 4.pdf

Click here to access/download **LaTeX Source Files**Figure 5.pdf

Click here to access/download **LaTeX Source Files**Figure6a.pdf

Click here to access/download **LaTeX Source Files**Figure6b.pdf

Click here to access/download **LaTeX Source Files**Figure7a.pdf

Click here to access/download **LaTeX Source Files**Figure7b.pdf

Click here to access/download **LaTeX Source Files**Figure8.pdf

Click here to access/download **LaTeX Source Files**Figure 9.pdf

Click here to access/download

LaTeX Source Files

Figure 10.pdf

Click here to access/download

LaTeX Source Files

Figure 11.pdf

Click here to access/download **LaTeX Source Files**Figure 12.pdf

Click here to access/download **LaTeX Source Files**Figure 13.pdf

Click here to access/download **LaTeX Source Files**numcompress.sty

Click here to access/download **LaTeX Source Files**Figure 14.pdf

Click here to access/download

LaTeX Source Files

Manuscript.tex

Click here to access/download **LaTeX Source Files**bibliography.bib

Supplementary Material

Click here to access/download **Supplementary Material**Supplementary Material.pdf

Journal of Sound and Vibration - Author Checklist

Authors should complete the following checklist and submit with their revised manuscript.

Math notation follows requirements on Guide for Authors (GFA) see:

✓

https://www.elsevier.com/journals/journal-of-sound-and-vibration/0022-460X/guide-for-authors	
Use Roman (normal upright) type for: Total differential operators (e.g. d in differential); i or j (square root of -1); exp or e (base of natural logarithms); Re or Im (real or imaginary part); log, In, sin, cos, etc.; abbreviations such as c.c. (complex conjugate); multiletter symbols (e.g. TL for transmission loss); subscripts of two or more letters identifiable as words or word-abbreviations (e.g., Apipe, fmax)	
For more unusual functions, JSV follows Abramowitz and Stegun's book. More detail given in the GFA (see link above).	
Unit symbols - These should be upright (e.g. kg, not kg).	
All authors are listed on the manuscript with correct affiliations, correct email address and are in correct order.	abla
Keywords present.	\square
Manuscript is not currently submitted to any other Journal.	\square
Six highlights are required, please note that each one should be no longer than 85 characters in length.	\square
Novelty of paper has been clearly stated in the Introduction.	abla
References are presented as per GFA.	abla
References not produced in English language to have English translation in brackets.	abla
Figures and Tables and Equations are numbered in sequence correctly. (See GFA).	abla
Nomenclature (if required) appears on second page of submission.	abla
Acknowledgements should appear in a separate section just after the conclusions.	\Box
All abbreviations, in both the abstract and main body of document, are defined once only, the first time they appear in the text. (N.B. The Abstract is treated as an independent text, where references are given in full and abbreviations and symbols, if used, are properly defined.)	
Figures – if there are multi-parts to a figures each part is labelled (a) (b) (c) etc. and the labels defined in th caption.	e figure
Figures – Colour can be used for the on-line version. Figures are reproduced in black and white in the printed ournal and must therefore be readable in both colour and black & white. (N.B. charges apply for production of colour figures in the printed journal)	
Appendices – should appear before the list of references and labelled A, B, C, (please see GFA for further information regarding equations, figures and tables in the appendices.	\square
Copyright – material reproduced from other publications (e.g. Tables, Figures), source is acknowledged.	
Please consider including your Twitter handle (if you have one).	

List of revisions

1. Page 4, Line: 81-84

"Though the periodic insertion of the cylindrical [33], cubic [34], and rod-like [28] resonators created band gaps to control Rayleigh wave propagation, the coupling between the resonator and the base material is not exploited in the design of the resonators."

(The structure of the paragraph (lines: 65-85) is slightly changed.)

2. Page 7, Line: 140-145

"Imposing the Neumann (traction-free) BCs ($\sigma_{33} = \sigma_{13} = 0$) on the surface of the half-space results in the well-known Rayleigh surface waves [37], whereas imposing the Dirichlet BCs ($u_1 = u_3 = 0$) results in nondispersive surface waves [35] that propagate with a phase speed of $c = \sqrt{c_L^2 + c_T^2}$. Next, let us evaluate the possible surface wave solutions for the following Cauchy type BCs that are of interest to this study:"

(A few details concerning the influence of Neumann and Dirichlet BCs on the possible surface wave solutions of the half-space are removed for brevity, based on the reviewer's suggestions.)

3. Page 20, Line: 390-393

"As the reflected Rayleigh wave is independent of the patch length, the amount of Rayleigh wave suppression achieved quantitatively represents the extent of mode-conversion of Rayleigh waves to bulk waves"

(This sentence is added based on the reviewer's suggestion.)

4. Page 28, Line: 489-494

"Though the physics behind Rayleigh wave interaction with the prismatic rods (considering only the longitudinal motion of resonators) is demonstrated analytically in [23] by solving the boundary value problem, the explanation to the mode-conversion of Rayleigh wave to shear waves is not explicitly detailed. This analysis provides an insight into the mechanism that leads to the conversion of Rayleigh waves to the bulk waves using prismatic resonators."

(This explanation is added to the manuscript in response to the reviewer's comments.)

5. Page 28, Fig. 14

(This figure is added to the draft in response to the reviewer's comments.)

6. Page 29, lines 506-518

"The FDFE analysis performed on a single resonator (Fig. 12(a)) can be extended to an array of 30 resonators to confirm the imposing of Mindlin BCs by all the resonators at the longitudinal resonance frequency. To demonstrate this, we compare the displacement fields resulting from the interaction of the Rayleigh wave with an array of resonators (Fig. 14(a)) and an array of an equal number of (frequency-independent) Mindlin BC patches (Fig. 14(b)) at 510 kHz (longitudinal resonance frequency of the

resonator). The dimensions of each Mindlin BC patch are identical to that of the resonator base and the spacing between the resonators/Mindlin BC patches is considered 1.4 mm ($\sim \lambda_R/4$). The displacement fields (Re(U₃)) for both the cases (resonators/patches) are very similar and show enhanced suppression of Rayleigh waves (90% suppression). These results indicate that an array of resonators impose an array of Mindlin BC patches (at 510 kHz) and thereby provide significant Rayleigh wave suppression"

(This is explanation is added for Fig.14. This figure has been added in response to the reviewer's comments)

7. Page 29, lines 520-524

"Although designing resonators based on longitudinal resonance frequency matching is straightforward, matching the BCs at the resonator base at prescribed frequencies could provide further insights into how the bandgaps are created leading to novel metasurface designs."

(The authors have added this sentence to the discussion section to highlight the novelty of the proposed BC-based metamaterial approach.)

8. Page 30, lines 557-559

"Analogous to the clamping of the vertical displacement by a prismatic resonator, non-intuitive resonator designs are possible through topology optimization that imposes Mindlin BCs at desired frequencies."

(The earlier statement in the conclusion is slightly modified.)

Credit Author Statement

Lalith Sai Srinivas Pillarisetti: Methodology, Software, Validation, Formal analysis, Investigation, Data Curation, Writing - Original Draft, Visualization.

Cliff J Lissenden: Conceptualization, Methodology, Writing - Review & Editing, Supervision, Project administration.

Parisa Shokouhi: Conceptualization, Methodology, Resources, Writing - Review & Editing, Supervision, Project administration, Funding acquisition.

Declaration of Interest Statement

Declaration of interests

oximes The authors declare that they have no known competing financial interests or personal relationships that could have appeared to influence the work reported in this paper.
☐The authors declare the following financial interests/personal relationships which may be considered as potential competing interests: